A thermo-mechanical model for variably saturated soils based on hypoplasticity

David Mašín, *Charles University in Prague, Czech Republic*
Nasser Khalili, *University of New South Wales, Sydney, Australia*

corresponding author:
David Mašín
Charles University in Prague
Faculty of Science
Albertov 6
12843 Prague 2, Czech Republic
E-mail: masin@natur.cuni.cz
Tel: +420-2-2195 1552, Fax: +420-2-2195 1556

May 9, 2011

Manuscript submitted to the
International Journal for Numerical and Analytical Methods in Geomechanics

Abstract

The paper presents a mechanical model for non-isothermal behaviour of unsaturated soils. The model is based on an incrementally non-linear hypoplastic model for saturated clays and can therefore tackle the non-linear behaviour of overconsolidated soils. A hypoplastic model for non-isothermal behaviour of saturated soils was developed and combined with the existing hypoplastic model for unsaturated soils based on the effective stress principle. Features of the soil behaviour that are included into the model, and those that are not, are clearly distinguished. The number of model parameters is kept to a minimum, and they all have a clear physical interpretation, to facilitate the model usefulness for practical applications. The step-by-step procedure used for the parameter calibration is described. The model is finally evaluated using a comprehensive set of experimental data for the thermo-mechanical behaviour of an unsaturated compacted silt.

Keywords: thermal effects; unsaturated soils; constitutive relationships; non-linearity; effective stress

1 Introduction

Understanding and modelling of thermo-mechanical properties of soils, particularly fine grained materials, has been the subject of many studies in the past. The possible reason for this attention is the non-isothermal conditions encountered in a number of high-priority applications such as nuclear waste disposal storage, buried high-voltage cables, pavements, and geothermal energy. When compared with the work on the mechanical and non-isothermal behaviour of saturated soils, the information on the thermo-mechanical behaviour of unsaturated soils is severely limited. As a result, researchers developing constitutive models for non-isothermal behaviour of unsaturated soil often rely on simple elastic-plastic models for saturated soils as the reference. However, these models have well-known drawbacks, particularly in their ability to capture the irreversible non-linear behaviour of overconsolidated soils. Such models then predict reversible elastic response before reaching large-strain Yield, whereas experimental data show gradual decrease of stiffness with strain level. In practical applications involving unsaturated soils, this can be of crucial importance since increasing suction induces an apparently overconsolidated state in the soil. For example, predictions of pressures imposed by the unsaturated compacted clay buffer onto the surface of nuclear storage containers depend primarily on the ability of the model to predict the non-linear behaviour of soils in an overconsolidated state. The aim of this paper is to provide a thermo-mechanical model for unsaturated soils, which predicts not only the qualitative effects of temperature and suction

on the soil behaviour at large strains, but also correctly captures the non-linear soil behaviour in the medium- to small-strain range. Temperature range in which the pore water is in liquid state is considered only. The number of model parameters is kept to a minimum to facilitate its practical applicability.

The first attempts to model non-isothermal soil behaviour were carried out within the field of saturated soil mechanics. The basic thermo-elasto-plastic framework, which is now well established, is attributed to the pioneering work by Hueckel and Baldi [28] and Hueckel and Borsetto [29]. They proposed a simple, yet conceptually powerful, approach to tackle the mechanical response of a soil exposed to variable heat conditions by defining the yield surface as a function of temperature as well as the plastic volumetric strain. In fact, most subsequent models are based on the same principle. Similar models to [28, 29] were developed in [44, 18]; Hueckel et al. [31] extended their model to soils with a cementation structure; Cui et al. [11] introduced independent thermal and mechanical yield mechanisms; Modaressi and Laloui [56] and Laloui and Cekerevac [42, 41] included a multi-mechanism plasticity allowing for predictions of a non-linear behaviour in shear; Abuel -Naga et al. [1] and Hueckel et al. [30] incorporated the temperature-dependent shape of the state boundary surface to accurately model the influence of temperature on the undrained stress path and peak shear strength.

Unlike some of the advanced models for the non-isothermal behaviour of saturated soils, the models for unsaturated soils are almost exclusively based on a single-surface Cam-clay-type elasto-plastic approach. Notable examples include the work of Francois and Laloui [15], Wu et al. [72] and Bolzon and Schrefler [6]. The first two models also include the water retention curve as part their formulations.

The structure of this paper is as follows: First, the relevant effects of temperature on the behaviour of saturated and unsaturated soils are summarised. Some contradictory experimental data are discussed and the features that are taken into account in the proposed model, and those that are not, are distinguished. Then, a thermo-mechanical model for non-isothermal soil behaviour is developed based on the framework of hypoplasticity, in particular on the model proposed by Mašín [48]. Subsequently, the newly developed model is combined with the existing hypoplastic model for unsaturated soils developed by Mašín and Khalili [54]. This is followed by a detailed step-by-step procedure for the calibration of the proposed constitutive model. The applicability of the model is evaluated on the basis of a comprehensive set of experimental data for the non-isothermal behaviour of unsaturated compacted silt given by Uchaipchat and Khalili [69].

Notations and Conventions: Compact tensorial notation is used throughout. Second-order tensors are denoted with bold letters (e.g. $\boldsymbol{\sigma}$, $\mathbf{N}$) and fourth-order tensors with calligraphic

bold letters (e.g. $\boldsymbol{\mathcal{L}}$, $\boldsymbol{\mathcal{A}}$). Symbols "$\cdot$" and ":" between tensors of various orders denote inner product with single and double contraction, respectively. The dyadic product of two tensors is indicated by "$\otimes$", and $\|\dot{\boldsymbol{\epsilon}}\|$ represents the Euclidean norm of $\dot{\boldsymbol{\epsilon}}$. The trace operator is defined as $\operatorname{tr}\dot{\boldsymbol{\epsilon}} = \mathbf{1} : \dot{\boldsymbol{\epsilon}}$; $\mathbf{1}$ and $\boldsymbol{\mathcal{I}}$ denote second-order and fourth-order unity tensors, respectively. Following the sign convention of continuum mechanics, compression is taken as negative. However, Roscoe's variables $p = -\operatorname{tr}\boldsymbol{\sigma}/3$ and $\epsilon_v = -\operatorname{tr}\boldsymbol{\epsilon}$, and pore fluid and gas pressures u_w and u_a are defined to be positive in compression. The operator $\langle x \rangle$ denotes the positive part of any scalar function x, thus $\langle x \rangle = (x + |x|)/2$.

2 Temperature effects on the mechanical behaviour of saturated and unsaturated soils

Comprehensive experimental data on the thermo-mechanical behaviour of unsaturated soils is scarce in the scientific literature [69, 61, 71]. On the other hand, a number of researchers have studied thermo-mechanical soil behaviour under saturated conditions. The following main characteristics of the thermal behaviour of soils appear to be the most important:

2.1 Compression behaviour under constant temperature

Temperature influences the normal compression lines (NCL) of a soil. NCL (corresponding to the actual soil structure and strain rate) represents maximum void ratio the soil can exist at for the given mean stress, it is thus a mean stress vs. void ratio trace of the state boundary surface (SBS), which is defined as a boundary of all possible states in the stress vs. void ratio space. A majority of the experimental data show that in the applied stress range the NCLs at different temperatures may be considered parallel to each other, while with increasing temperature the specific volume at the NCL for the given effective mean stress p decreases [69, 9, 10, 7]. Though a number of research studies show a constant slope of NCL with temperature, exceptions have also been reported [67, 61]. In all the cases, however, an increase in temperature leads to a decreases in the apparent preconsolidation stress. A number of experiments by different authors has been evaluated by Laloui and Cekerevac [40], who observed a linear decrease in the preconsolidation stress with the logarithm of temperature.

A few experimental studies contradict this general trend and indicate a higher position of the NCLs for higher temperatures, thus showing an increase in the size of the SBS with temperature [65]. The discrepancy is believed to be caused by the manner in which the

initial void ratio was evaluated. Khalili et al. [36] have shown that heating overconsolidated soil samples leads to expansion volumetric strains, but the void ratio remains essentially constant (see Sec. 2.3). Then, if the void ratio is calculated from resultant volumetric strain using a standard procedure, the calculated void ratio will be higher than the actual one, and this may lead to an apparent discrepancy in the relative position of normal compression lines.

The model presented in this paper allows for variable positions and slopes of NCLs with temperature. However, in agreement with the majority of the published experimental data, the size of the state boundary surface is always considered to decrease with increasing temperature.

2.2 Behaviour in shear under constant temperature

The experimental evidence of the influence of temperature on the soil peak strength is contradictory, as is discussed below. However, most results agree that the critical state friction angle is independent of temperature [69, 31, 28, 45, 67, 10, 1].

Variation of the peak strength with temperature appears to be dependent on the soil being tested. Some authors report a decrease in the peak strength of overconsolidated soil with increasing temperature [69, 31, 28, 45, 12]; this decrease may be explained consistently within the constitutive framework developed by Hueckel and Baldi [28], that increasing temperature decreases the apparent overconsolidation ratio (OCR). As the peak strength is known to depend on OCR, decreasing apparent OCR leads to a decrease in the peak strength.

Contradictory to this behaviour, however, an increase in the peak shear strength and a decrease of the apparent preconsolidation pressure with temperature has been reported by some authors [67, 27, 1, 10, 39]. In some cases, the difference may be attributed to the different initial states of the specimens at different temperatures and the results may still be explained using the Hueckel and Baldi [28] framework. In other cases (e.g. when the soil is in a normally consolidated condition), however, such an approach fails to explain this phenomenon. A consistent treatment of this problem has been proposed by Abuel-Naga et al. [1], who considered the temperature-dependent shape of the state boundary surface, while keeping, in agreement with the majority of experimental data, the critical state friction angle constant. In fact, a similar interpretation was indirectly proposed earlier by Graham et al. [18], who imposed a variable shape for the constant-void-ratio cross-section through the SBS by changing the elastic compressibility parameter κ. Finally, concurrently with Abuel-Naga et al. [1], Hueckel et al. [30] also proposed a variable shape of the SBS with temperature to tackle this problem. However, Hueckel et al. [30] imposed variation of the shape of the SBS by

altering the critical state friction angle, rather than by introducing the additional parameter controlling the shape of SBS, which appears to contradict the available experimental data (see above).

The model presented in this paper only allows for the control of the size of the SBS with temperature, while the shape of the SBS is independent of temperature. Incorporating a variable shape of the SBS with temperature would require further enhancement of the model.

2.3 Soil response due to variation in temperature

It is generally agreed that the soil response to heating-cooling cycles is strongly dependent on the apparent overconsolidation ratio. At high OCRs, the soil response is essentially reversible, thus, there are no permanent changes in the soil structure. As discussed in detail by Khalili et al. [36], this type of response is controlled solely by the thermal expansion coefficient of the solid particles, independent of the soil porosity. An interesting consequence of this fact is that heating or cooling of overconsolidated soils imposes no change in the porosity [36]. This has not generally been reported by researchers, as they typically calculate a change in porosity using the amount of water expelled from the sample and do not take into account the thermal expansion of the water itself. The available experimental data also demonstrates that the thermal expansion coefficient, α_s, of the soil skeleton may essentially be considered as independent of the effective stress and temperature [69, 13, 65, 2]. Some authors, however, consider the slight dependency of α_s on the state variables in the constitutive models [42].

As indicated in the previous paragraph, the response of a soil at high OCRs is generally reversible. At low OCRs, however, the mechanisms controlling the heating and cooling responses are substantially different. Upon cooling, the state boundary surface increases in size (see Sec. 2.1); the soil structure is thus not exposed to meta-stable conditions, and consequently the volumetric response is the result of the thermal contraction of the soil particles, which does not depend on the overconsolidation ratio [69, 13, 65]. In contrast, a reduction of the size of SBS due to heating imposes irreversible changes of the open structure of a soil at low OCR, leading to the so-called heating-induced collapse. In general, the collapsible strains due to heating of a soil at low OCRs are significantly larger than the straining imposed by the expansion of soil particles, and they are controlled by the relative position of the normal compression lines at different temperatures. The collapse due to heating is not an abrupt process that activates once the soil state reaches the SBS; instead, its influence gradually increases with decreasing OCR, as demonstrated in a number of experimental studies [13, 28, 4, 65, 14]. Demars and Charles [14] also evaluated the permanent volume change (and thus differences in NCLs) due to temperature cycling and related it to the soil plasticity.

In general, there are two features of the thermal behaviour of soils reported in the literature that appear to contradict the consistent framework presented above. First, some authors report expansion behaviour upon cooling [28, 18]. This behaviour could be due to an artifact of the experimental procedures involved in testing: One possible explanation is the development of water vapor at high temperatures within the soil specimens. If the temperature decrease is rapid, existence of water vapor and its reduction in volume will draw water into the specimen, which in turn may be interpreted as the expansion of the sample. Cui et al. [11] explained this phenomenon by the dependency of the soil behaviour on the rate of application of the thermal gradient. Second, several authors have reported the apparent oveconsolidation of initially normally consolidated soil specimens after heating [65, 68] or after a heating-cooling cycle [7]. In the case of the heating-cooling cycle, this phenomenon may be fully explained by the framework presented above, but it does not explain the overconsolidation effect induced by pure heating. To account for this effect, Cui et al. [11] developed a two-mechanism plasticity model distinguishing between thermal (TY) and mechanical (LY) yielding. This quasi-overconsolidation effect may also be explained by a creep straining that occurrs during the slow heating process. As demonstrated by Burghignoli et al. [7] among others, creep has a similar effect on quasi-preconsolidation as the effect observed in heating tests by Sultan et al. [65] and Towhata et al. [68].

The model presented in this paper considers the volume change due to cooling and heating of overconsolidated soil to be a fully reversible process governed by a constant value of the thermal expansion coefficient α_s. Heating-induced collapse is an irreversible process controlled by the position of NCLs and its effect gradually increases with decreasing distance from the SBS. In light of the explanation above, cooling expansion and heating induced quasi-overconsolidation are not treated by any additional thermal mechanisms.

3 Reference hypoplastic model for saturated soils

Hypoplasticity is a particular class of incrementally non-linear constitutive models for soils developed independently at the Universities of Karlsruhe and Grenoble (see [66]). Unlike the elasto-plastic models, the strain rate is not decomposed into reversible (elastic) and irreversible (plastic) parts, and the incrementally non-linear character of the soil behaviour is reproduced by the general equation for the stress rate, which is non-linear in the strain rate $\dot{\boldsymbol{\epsilon}}$. The reference model for the present derivations was proposed by Mašín [48] and it is based on the Karlsruhe approach to hypoplasticity [70, 58, 25]. Within this context, the

stress-strain rate relationship is written as [21]

$$\mathring{\boldsymbol{\sigma}} = f_s \left(\boldsymbol{\mathcal{L}} : \dot{\boldsymbol{\epsilon}} + f_d \mathbf{N} \| \dot{\boldsymbol{\epsilon}} \| \right) \tag{1}$$

where $\mathring{\boldsymbol{\sigma}}$ denotes the objective (Zaremba-Jaumann, see [38]) rate of the effective stress tensor, $\dot{\boldsymbol{\epsilon}}$ is the Euler's stretching tensor, $\boldsymbol{\mathcal{L}}$ and $\mathbf{N}$ are fourth- and second-order constitutive tensors and f_s and f_d are two scalar factors, denoted as *barotropy* and *pyknotropy* factors respectively. A detailed description of these factors and the mathematical structure of the model is outside the scope of this paper and the readers are referred to the relevant publication [48].

The model is conceptually based on critical state soil mechanics (see Gudehus and Mašín [23]) and its five parameters (φ_c, N, λ^*, κ^*, r) have a similar physical interpretation as the parameters of the Modified Cam clay model [62]. Parameters N and λ^* define the position and the slope of the isotropic normal compression line, following the formulation by Butterfield [8]

$$\ln(1+e) = N - \lambda^* \ln \frac{p}{p_r} \tag{2}$$

where p_r is an arbitrary reference stress, which is considered equal to 1 kPa throughout this paper. The parameters N and λ^* also control the position of the critical state line, with the assumed formulation

$$\ln(1+e) = N - \lambda^* \ln \frac{p}{2p_r} \tag{3}$$

The next parameter, κ^*, controls the slope of the isotropic unloading line and the parameter r the shear stiffness. Finally, φ_c is the critical state friction angle, that controls the size of the critical state locus in the stress space, defined by the formulation given in Matsuoka and Nakai [47]. The model considers the void ratio e as a state variable. The model is capable of predicting the non-linear soil behaviour in the medium- to large-strain range. In order to predict the small- to very-small strain stiffness behaviour, the basic formulation (1) must be enhanced by the so-called intergranular strain concept [59]. For brevity, this extension will not be presented here, but it can be applied to the proposed thermo-mechanical model for unsaturated soils. However, additional experimental investigation into the influence of temperature on the very small strain behaviour would be needed.

The reference model is conceptually simple and, due to the small number of material parameters and a simple calibration procedure, it is easy to use in practical applications. It has been shown to provide accurate predictions of non-linear soil behaviour on both the element level [55, 24, 51] and boundary value problem level [50, 22]. The model was studied in greater detail by Mašín and Herle [53], who demonstrated that implicit in the model formulation is the existence of a state boundary surface whose form and size can be analytically expressed.

These derivations were crucial for further development of the model [49, 54], and also allow for its extension to the thermal effects, presented in this paper.

4 Thermomechanical model for saturated soils

To account for the influence of temperature on the apparent preconsolidation and the size of the state boundary surface, the model parameters controlling the position and slope of the normal compression line N and λ^* (Eq. (2)) are considered to be dependent on temperature. The normal compression line thus has the following formulation:

$$\ln(1+e) = N(T) - \lambda^*(T) \ln \frac{p}{p_r} \tag{4}$$

In principle, any dependency of $N(T)$ and $\lambda^*(T)$ on T may considered. The following relation is adopted in the present work:

$$N(T) = N + n_T \ln\left(\frac{T}{T_0}\right) \qquad\qquad \lambda^*(T) = \lambda^* + l_T \ln\left(\frac{T}{T_0}\right) \tag{5}$$

in which T_0 is a reference temperature, and the values of $N(T)$ and $\lambda^*(T)$ corresponding to the reference temperature $N(T_0)$ and $\lambda^*(T_0)$ are model parameters, which are for brevity denoted as N and λ^*. n_T and l_T are additional parameters controlling the influence of temperature on NCL. It is noted that according to the experimental evidence, the slope of the NCL for most practical problems may be taken as independent of temperature (thus $l_T = 0$). This means that, in order to predict a decrease of the preconsolidation pressure with increasing temperature, n_T should be negative. Eq. (5) can approximately predict a linear dependency of the apparent preconsolidation pressure on the logarithm of temperature. Such a dependency was observed by Laloui and Cekerevac [40] based on the experimental data of several authors.

When the overconsolidated saturated soil, which is not prone to heating-induced collapse of the soil structure, is heated under drained conditions, it undergoes thermal expansion. Khalili et al. [36] have shown that the overall thermal expansion coefficient of a porous medium α_s is solely controlled by, and is equal to, the thermal expansion coefficient of the solid constituent. It follows that the thermal expansion is independent of the void ratio, has no effect on the void ratio, and is fully reversible. The available experimental data also shows that the coefficient α_s may essentially be considered as independent of the effective stress

and temperature [69, 13, 65, 2]. We assume a thermally isotropic material, thus:

$$\dot{\boldsymbol{\epsilon}}^{TE} = \frac{\mathbf{1}}{3}\alpha_s \dot{T} \tag{6}$$

where $\mathbf{1}$ is a unit second-oder tensor. To account for the full reversibility of the $\dot{\boldsymbol{\epsilon}}^{TE}$ strain rate, the hypoplastic formulation (1) is modified in the following way:

$$\mathring{\boldsymbol{\sigma}} = f_s \left[\boldsymbol{\mathcal{L}} : (\dot{\boldsymbol{\epsilon}} - \dot{\boldsymbol{\epsilon}}^{TE}) + f_d \mathbf{N} \| \dot{\boldsymbol{\epsilon}} - \dot{\boldsymbol{\epsilon}}^{TE} \| \right] \tag{7}$$

The reversible component of the thermal strain rate does not imply any change in the void ratio of the porous medium. To account for this phenomenon, the rate of the void ratio is not calculated solely from the total strain rate $\dot{\boldsymbol{\epsilon}}$, but it is given by

$$\dot{e} = (1 + e)\,\mathrm{tr}\,(\dot{\boldsymbol{\epsilon}} - \dot{\boldsymbol{\epsilon}}^{TE}) \tag{8}$$

In addition to the reversible strains induced by the volumetric change of the solid constituents, a soil with a high void ratio (low overconsolidation ratio) is prone to heating-induced irreversible compression of the soil structure. In terms of critical state soil mechanics, this is manifested by the reduction of the size of the state boundary surface. As demonstrated by Mašín and Khalili [54], collapse of the soil structure at constant effective stress may be incorporated into hypoplasticity through an additional tensorial term $\mathbf{H}$. For the states at the state boundary surface, the collapsible term due to heating $\mathbf{H}_T$ is incorporated by

$$\mathring{\boldsymbol{\sigma}} = f_s \left[\boldsymbol{\mathcal{L}} : (\dot{\boldsymbol{\epsilon}} - \dot{\boldsymbol{\epsilon}}^{TE}) + f_d \mathbf{N} \| \dot{\boldsymbol{\epsilon}} - \dot{\boldsymbol{\epsilon}}^{TE} \| \right] + \mathbf{H}_T \tag{9}$$

The calculation of $\mathbf{H}_T$ follows from the requirement that when the normally consolidated soil is heated under constant effective stress, its state must remain on the state boundary surface. In other words, stress normalised by the size of the state boundary surface ($\boldsymbol{\sigma}_n$) must not change. The size of the state boundary surface is measured by the Hvorslev equivalent pressure p_e on the normal compression line, which follows from (4):

$$p_e = p_r \exp\left[\frac{N(T) - \ln(1 + e)}{\lambda^*(T)} \right] \tag{10}$$

The rate of the normalised stress state $\boldsymbol{\sigma}_n = \boldsymbol{\sigma}/p_e$ is given by

$$\mathring{\boldsymbol{\sigma}}_n = \frac{\mathring{\boldsymbol{\sigma}}}{p_e} - \frac{\boldsymbol{\sigma}}{p_e^2}\dot{p}_e \tag{11}$$

and the rate of the Hvorslev equivalent pressure $\dot{p}_e$ follows from (10):

$$\dot{p}_e = -\frac{p_e}{\lambda^*(T)} \operatorname{tr} \dot{\boldsymbol{\epsilon}} + \frac{\partial p_e}{\partial T} \dot{T} \tag{12}$$

As already indicated, heating of the soil whose state lies at the state boundary surface must impose no change in $\boldsymbol{\sigma}_n$. Combination of (11) with (12) thus yields

$$\mathring{\boldsymbol{\sigma}} = -\frac{\boldsymbol{\sigma}}{\lambda^*(T)} \operatorname{tr} \dot{\boldsymbol{\epsilon}} + \frac{\boldsymbol{\sigma}}{p_e} \frac{\partial p_e}{\partial T} \dot{T} \tag{13}$$

The basic hypoplastic model is characterised by $\partial p_e / \partial T = 0$. It thus follows that the relation

$$\mathring{\boldsymbol{\sigma}} = -\frac{\boldsymbol{\sigma}}{\lambda^*(T)} \operatorname{tr} \dot{\boldsymbol{\epsilon}} \tag{14}$$

gives the effective stress rate predicted by the basic hypoplastic model for compression paths along NCL. In general, this rate is given by Eq. (7). We thus can write

$$\mathring{\boldsymbol{\sigma}} = f_s \left[\boldsymbol{\mathcal{L}} : (\dot{\boldsymbol{\epsilon}} - \dot{\boldsymbol{\epsilon}}^{TE}) + f_d \mathbf{N} \| \dot{\boldsymbol{\epsilon}} - \dot{\boldsymbol{\epsilon}}^{TE} \| \right] + \frac{\boldsymbol{\sigma}}{p_e} \frac{\partial p_e}{\partial T} \dot{T} \tag{15}$$

Comparison of (15) with (9) then yields the expression for the term $\mathbf{H}_T$:

$$\mathbf{H}_T = \frac{\boldsymbol{\sigma}}{p_e} \frac{\partial p_e}{\partial T} \dot{T} \tag{16}$$

For the particular choice of the dependency of $N(T)$ and $\lambda^*(T)$ on temperature (5), we have

$$\mathbf{H}_T = \frac{\boldsymbol{\sigma}}{T \lambda^*(T)} \left[n_T - l_T \ln \frac{p_e}{p_r} \right] \dot{T} \tag{17}$$

Eqs. (17) and (9) define the thermo-mechanical hypoplastic model for normally consolidated conditions under constant temperature or during heating ($\dot{T} \geq 0$). In order to generalise it for an arbitrary state and arbitrary loading conditions, it must be enhanced in the following way:

1. Collapse of the soil structure is an irreversible process that takes place during heating only. Upon cooling, volumetric contraction of the soil skeleton is controlled solely by the thermal contraction of the solid particles. Thus, the $\mathbf{H}_T$ term is active only for $\dot{T} \geq 0$, and Eq. (17) can be rewritten as

$$\mathbf{H}_T = \frac{\boldsymbol{\sigma}}{T \lambda^*(T)} \left[n_T - l_T \ln \frac{p_e}{p_r} \right] \langle \dot{T} \rangle \tag{18}$$

2. Collapse of the soil structure is most pronounced for a soil with an open structure, i.e. soil at low overconsolidation ratios. Thus, the influence of the $\mathbf{H}_T$ term should vanish with increasing OCR. To reflect this, Mašín and Khalili [54] introduced a factor f_u which has the following property: $f_u = 1$ for $OCR = 1$ and $f_u \to 0$ for $OCR \to \infty$. The factor f_u multiplies the term $\mathbf{H}_T$ in the model formulation, and thus reduces its effect with increasing overconsolidation ratio:

$$\mathring{\boldsymbol{\sigma}} = f_s \left[\boldsymbol{\mathcal{L}} : (\dot{\boldsymbol{\epsilon}} - \dot{\boldsymbol{\epsilon}}^{TE}) + f_d \mathbf{N} \| \dot{\boldsymbol{\epsilon}} - \dot{\boldsymbol{\epsilon}}^{TE} \| \right] + f_u \mathbf{H}_T \tag{19}$$

The following expression satisfies the outlined properties of the factor f_u:

$$f_u = \left(\frac{p}{p^{SBS}} \right)^m \tag{20}$$

where p^{SBS} is the effective mean stress at the SBS corresponding to the projection of the stress state from the stress origin onto the SBS at current void ratio e. m is a model parameter controlling the influence of overconsolidation on the heating-induced collapse. The expression for f_u may be derived from the formulation of the pyknotropy factor f_d of the basic hypoplastic model:

$$f_d = \left(\frac{2p}{p_e} \right)^\alpha \tag{21}$$

Combining of (21) with (20) leads to

$$\frac{p}{p^{SBS}} = \left(\frac{f_d}{f_d^{SBS}} \right)^{1/\alpha} \tag{22}$$

where f_d^{SBS} is the value of the pyknotropy factor f_d calculated for a state boundary surface passing through the current stress point. An analytical expression for f_d^{SBS} has been derived in Reference [53]

$$f_d^{SBS} = \| f_s \boldsymbol{\mathcal{A}}^{-1} : \mathbf{N} \|^{-1} \tag{23}$$

where the fourth-order tensor $\boldsymbol{\mathcal{A}}$ is given by

$$\boldsymbol{\mathcal{A}} = f_s \boldsymbol{\mathcal{L}} - \frac{1}{\lambda^*(T)} \boldsymbol{\sigma} \otimes \mathbf{1} \tag{24}$$

Therefore, the expression for the factor f_u reads

$$f_u = \left[f_d \| f_s \boldsymbol{\mathcal{A}}^{-1} : \mathbf{N} \| \right]^{m/\alpha} \tag{25}$$

The influence of the parameter m on the value of the factor f_u is clear from Fig. 1. For high values of m, collapse takes place very close to the state boundary surface only, and inside the SBS the thermally-induced strains are fully reversible. With decreasing value of m, the collapse takes place at progressively higher overconsolidation ratios.

[Figure 1 about here.]

3. The factor $\mathbf{H}_T$ defined by Eq. (18) satisfies the requirement of consistency of the model predictions at the SBS. However, the amount of collapse predicted by the model from Eq. (19) decreases with increasing OCR even for $m = 0$ (and thus $f_u = 1$). This property was found to be undesirable, since with (18) it is not possible to fully control the collapsible strains by the parameter m. In fact, the model defined using $\mathbf{H}_T$ by Eq. (18) may overpredict the collapse potential with increasing OCR even for $m = 0$. To overcome this shortcoming, the factor $\mathbf{H}_T$ is modified for higher OCRs such that the amount of collapse for $m = 0$ (and thus $f_u = 1$) is independent of the overconsolidation ratio. The value $m = 0$ is then a physical limit for possible values of m, and for natural soils m would indeed be higher then 0.

   For $f_u = 1$, $\mathring{\boldsymbol{\sigma}} = \mathbf{0}$ and $\dot{T} >= 0$ the formulation of the model (19) reads

$$-\mathbf{H}_T = f_s \left[\boldsymbol{\mathcal{L}} : (\dot{\boldsymbol{\epsilon}} - \dot{\boldsymbol{\epsilon}}^{TE}) + f_d \mathbf{N} \| \dot{\boldsymbol{\epsilon}} - \dot{\boldsymbol{\epsilon}}^{TE} \| \right] \tag{26}$$

   We now wish to modify the left-hand side of Eq. (26) in such a way that the volumetric response due to heating is independent of OCR. To achieve this, we multiply the left-hand side of Eq. (26) by a yet-unknown factor c_i. We thus have

$$-c_i \mathbf{H}_T = f_s \left[\boldsymbol{\mathcal{L}} : (\dot{\boldsymbol{\epsilon}} - \dot{\boldsymbol{\epsilon}}^{TE}) + f_d \mathbf{N} \| \dot{\boldsymbol{\epsilon}} - \dot{\boldsymbol{\epsilon}}^{TE} \| \right] \tag{27}$$

   The factor c_i is evaluated based on the isotropic formulation of the model. After algebraic manipulation, detailed in Appendix 2, we finally obtain the following isotropic form of (27)

$$c_i \frac{\mathrm{tr}(\mathbf{H}_T)}{3} = -\frac{p}{\lambda^*(T)} \left[\frac{3 + a^2 - f_d a \sqrt{3}}{3 + a^2 - 2^\alpha a \sqrt{3}} \right] \frac{\dot{e}}{1 + e} \tag{28}$$

   Scalars a and α are defined in the Appendix 1.

For the state at the state boundary surface, the following properties of Eq. (28) hold: First, $c_i = 1$ (Eq. (26), which assume $c_i = 1$, has originally been derived for states at the SBS). Second, for states at the SBS $f_d = f_d^{SBS}$ (f_d^{SBS} was defined in Eq. (23)). For states at the SBS we thus have

$$\frac{\mathrm{tr}(\mathbf{H}_T)}{3} = -\frac{p}{\lambda^*(T)} \left[\frac{3 + a^2 - f_d^{SBS} a\sqrt{3}}{3 + a^2 - 2^\alpha a\sqrt{3}} \right] \frac{\dot{e}}{1+e} \tag{29}$$

Comparing (29) with (28) leads us to

$$c_i = \frac{3 + a^2 - f_d a\sqrt{3}}{3 + a^2 - f_d^{SBS} a\sqrt{3}} \tag{30}$$

The factor c_i may be incorporated into the definition of the term $\mathbf{H}_T$, which now reads

$$\mathbf{H}_T = c_i \frac{\boldsymbol{\sigma}}{T\lambda^*(T)} \left[n_T - l_T \ln \frac{p_e}{p_r} \right] \langle \dot{T} \rangle \tag{31}$$

The general rate formulation of the model is given by Eq. (19).

When compared with the reference hypoplastic model for constant temperature, the new model requires specification of additional parameters n_T and l_T (for temperature dependent NCL), α_s (thermal skeletal expansion coefficient), parameter m controlling the distance from the SBS upon which heating collapse takes place, and the reference temperature T_0. The model considers one additional state variable (temperature T). Evaluation of the material parameters is detailed in Sec. 6.

5 Adaptation of the model to unsaturated states

Experimental evidence shows that the temperature does not change the *qualitative* response of an unsaturated soil to a change in suction, and that suction does not change the *qualitative* response of the soil exposed to a change in temperature. Thanks to this property, constitutive models for the effects of unsaturation and temperature may be combined in a hierarchical way, in a sense defined by Muir Wood and Gajo [57]. In this section we take advantage of this fact, and combine the model for temperature effects proposed in Sec. 4 with a hypoplastic mechanical model for unsaturated soils proposed by Mašín and Khalili [54].

Central to the present model is the notion of effective stress, which describes the overall effect of external forces and pore fluids on the macroscopic stress of the solid skeleton [35, 46]. It is

recognised that different terms are suggested by different authors for this stress entity (such as average skeleton stress [17] or intergranular stress [32]). In addition to the effective stress variable, a second (typically scalar) variable is needed to describe the stiffening effect of water menisci on the soil structure. In the context of critical state soil mechanics [63], this controls the size of state boundary surface. The matric suction s is typically considered as this scalar stress variable (and it will be used throughout this paper), though different alternatives have been put forward in the literature [26, 43], including the function of a degree of saturation (Gallipoli et al. [17]).

The effective stress in unsaturated soils $\boldsymbol{\sigma}$ may in general be written as

$$\boldsymbol{\sigma} = \boldsymbol{\sigma}^{tot} + \chi u_w \mathbf{1} + (1-\chi) u_a \mathbf{1} = \boldsymbol{\sigma}^{net} - \chi s \mathbf{1} \tag{32}$$

where $\boldsymbol{\sigma}^{tot}$ is a total stress, u_a is the pore air pressure and u_w is the pore water pressure, $\boldsymbol{\sigma}^{net}$ is the net stress defined as $\boldsymbol{\sigma}^{net} = \boldsymbol{\sigma}^{tot} + u_a \mathbf{1}$ and s is matric suction $s = u_a - u_w$. χ is the Bishop [5] effective stress factor. The incremental form of (32) is written as

$$\dot{\boldsymbol{\sigma}} = \dot{\boldsymbol{\sigma}}^{net} + \psi \dot{u}_w \mathbf{1} + (1-\psi) \dot{u}_a \mathbf{1} = \dot{\boldsymbol{\sigma}}^{net} - \psi \dot{s} \mathbf{1} \tag{33}$$

where

$$\psi = \frac{d(\chi s)}{ds} \tag{34}$$

A suitable empirical expression for the effective stress, which was shown to be capable of predicting both the volume changes and shear strength behaviour of unsaturated soils, was proposed by Khalili and Khabbaz [35] and Khalili et al. [33]. They have related the factor χ to suction and to the suction at the transition between saturated and unsaturated states s_e by

$$\chi = \begin{cases} 1 & \text{for} \quad s < s_e \\ \left(\dfrac{s_e}{s}\right)^{\gamma} & \text{for} \quad s \geq s_e \end{cases} \tag{35}$$

A combination of (35) and (34) yields an expression for ψ, which is equal to $\psi = (1-\gamma)\chi$ for $s \geq s_e$ and $\psi = 1$ otherwise.

Khalili and Khabbaz [35] have shown that the best-fit value of the exponent $\gamma = 0.55$ is suitable to represent the behaviour of different soil types. γ can thus be considered as a material independent constant. Unlike the exponent γ, however, s_e depends on the soil type (see [16] for overview). In addition, it is dependent on the suction path (i.e. whether the state is on the drying, wetting or scanning branch of the water retention curve) and on the soil state, quantified by the void ratio and temperature.

In the model by Mašín and Khalili [54], the influence of suction on the state boundary surface is considered by means of the dependency of $N(s)$ and $\lambda^*(s)$ on suction. When combined with the model for temperature effects from Sec. 2, the expression for the isotropic normal compression line reads

$$\ln(1+e) = N(s,T) - \lambda^*(s,T) \ln \frac{p}{p_r} \tag{36}$$

with

$$N(s,T) = N + n_s \left\langle \ln \frac{s}{s_e} \right\rangle + n_T \ln\left(\frac{T}{T_0}\right) \qquad \lambda^*(s,T) = \lambda^* + l_s \left\langle \ln \frac{s}{s_e} \right\rangle + l_T \ln\left(\frac{T}{T_0}\right) \tag{37}$$

The parameters n_s and l_s describe the effect of suction on the position and slope of NCL. $N = N(0,T_0)$ and $\lambda^* = \lambda^*(0,T_0)$ are model parameters.

Unlike the effect of reversible strains due to variable temperature in the model from Sec. 4, straining of overconsolidated soil due to variable suction does not need to be considered separately in the proposed model. This is because of the definition of the effective stress, which changes with matric suction and implies the same response of the soil skeleton as the variation of the net stress under constant suction [33]. In addition to these phenomena, however, wetting of a soil with an open structure causes irreversible changes to the soil structure. To reflect this, a wetting-induced collapse term $\mathbf{H}_s$ is included in the general model formulation (19):

$$\mathring{\boldsymbol{\sigma}} = \mathring{\boldsymbol{\sigma}}^{net} - \psi \dot{s} \mathbf{1} = f_s \left[\boldsymbol{\mathcal{L}} : (\dot{\boldsymbol{\epsilon}} - \dot{\boldsymbol{\epsilon}}^{TE}) + f_d \mathbf{N} \| \dot{\boldsymbol{\epsilon}} - \dot{\boldsymbol{\epsilon}}^{TE} \| \right] + f_u \left(\mathbf{H}_s + \mathbf{H}_T \right) \tag{38}$$

where derivation of the $\mathbf{H}_s$ term follows conceptually the same approach as the derivation of the term $\mathbf{H}_T$ in Sec. 4. Finally, we obtain

$$\mathbf{H}_s = -c_i \frac{\boldsymbol{\sigma}}{s \lambda^*(s,T)} \left[n_s - l_s \ln \frac{p_e}{p_r} \right] \langle -\dot{s} \rangle \tag{39}$$

valid for $s \geq s_e$ and $\mathbf{H}_s = \mathbf{0}$ otherwise.

Note that the same factor f_u is here, for the sake of simplicity and due to the lack of detailed experimental data, introduced to control the influence of OCR on both wetting- and thermally-induced collapse. There appears to be no conclusive experimental evidence supporting this simplifying choice, however. If needed, f_u factor can be split into two parts, one controlling the wetting-induced collapse and the second controlling the thermally -induced

collapse. Eq. (38) would then read

$$\mathring{\boldsymbol{\sigma}} = \mathring{\boldsymbol{\sigma}}^{net} - \psi \dot{s}\mathbf{1} = f_s \left[\boldsymbol{\mathcal{L}} : (\dot{\boldsymbol{\epsilon}} - \dot{\boldsymbol{\epsilon}}^{TE}) + f_d \mathbf{N} \| \dot{\boldsymbol{\epsilon}} - \dot{\boldsymbol{\epsilon}}^{TE} \| \right] + f_{us} \mathbf{H}_s + f_{uT} \mathbf{H}_T \tag{40}$$

with

$$f_{us} = \left[f_d \| f_s \boldsymbol{\mathcal{A}}^{-1} : \mathbf{N} \| \right]^{m_s/\alpha} \qquad \text{and} \qquad f_{uT} = \left[f_d \| f_s \boldsymbol{\mathcal{A}}^{-1} : \mathbf{N} \| \right]^{m_T/\alpha} \tag{41}$$

and two model parameters m_s and m_T. In the present evaluation, however, we keep the simpler form (38).

Note also that the factor c_i was not included in the original formulation of the model for unsaturated soils from [54]. The parameter m has thus a slightly different influence on the rate of wetting-induced collapse than in the original model for unsaturated soils.

With Eqs. (36) - (39), the thermo-mechanical model for saturated soils from Sec. 4 is adapted to unsaturated states. The complete model requires in addition to the model from Sec. 4 specification of parameters s_e, n_s and l_s. A complete mathematical formulation of the model (including components of the reference hypoplastic model) is detailed in the Appendix 1. The calibration of the model parameters is described in detail in the next section. It is based on a complete set of experimental data for the thermo-mechanical behaviour of an unsaturated compacted silt given by Uchaipchat and Khalili [69].

Note that in the evaluation of the model in Sec. 7, s_e is considered as a material constant, but, as already indicated, it depends on a number of variables. The dependency of s_e on different aspects may be incorporated into the proposed model by following the approaches proposed by different researchers. The influence of the hydraulic hysteresis on the value of s_e (and on the effective stress factor χ in general) was studied by Khalili et al. [34] and Khalili and Zargarbashi [37]. The expression for the influence of the void ratio on s_e, based on the effective stress equation from (35), was proposed by Mašín [52]. Finally, the dependency of s_e on temperature may be incorporated by means of an approach proposed by Grant and Salezdaleh [20], which has been thoroughly evaluated by means of comparison with the experimental data on soil water retention behaviour under variable temperatures [19, 3, 64, 60].

6 Determination of the model parameters

First, the parameter s_e needed to calculate the effective stress in simulations of the other tests has to be selected. For the sake of simplicity, in the present evaluation it is considered as a material constant. The value $s_e = 18$ kPa, evaluated by Uchaipchat and Khalili [69] from the position of water retention curve at $T = 25°C$, was considered as the most appropriate. Calibration of s_e was followed by calibration of the parameters controlling NCL and isotropic mechanical response of saturated soil (N, λ^*, κ^*) and position and slope of NCL of unsaturated and heated soil (n_s, l_s, n_T and l_T). At this point it is possible to simulate the constant s and constant T shear experiments, which were used to calibrate the shear stiffness parameter r and the critical state friction angle φ_c. Finally, the thermal heating test of an overconsolidated soil was used to calibrate the skeletal thermal expansion coefficient α_s and heating- and wetting-induced collapse parameter m.

6.1 Parameters controlling the isotropic mechanical response at constant s and T

As noted by Uchaipchat and Khalili [69], the slopes of the normal compression lines for the tested silt were independent of suction and temperature for the stress range of interest. Figure 2 shows the results of several constant suction and constant temperature isotropic compression tests, plotted in the effective stress space. All the NCLs can be approximated by a linear representation in the $\ln p$ vs. $\ln(1 + e)$ plane with a unique slope of $\lambda^* = 0.06$. The independency of λ^* on T and s leads to $l_s = 0$ and $l_T = 0$.

[Figure 2 about here.]

Unlike the slope λ^*, the intercept N is clearly dependent on s and T. Its value for the reference temperature T_0 and $s = 0$ is $N = 0.772$. The dependency of $N(s, T)$ on the values of $\ln(s/s_e)$ and $\ln(T/T_0)$, used for evaluation of the parameters n_s and n_T, is shown in Fig. 3 and leads to $n_s = 0.0035$ and $n_T = -0.01$. Note that there appears to be no clear cross-dependency between temperature and suction effects, i.e. n_T is not obviously dependent on suction, and n_s does not appear to be systematically dependent on temperature. The reference temperature is considered to be $T_0 = 25°C$.

[Figure 3 about here.]

Uchaipchat and Khalili [69] have demonstrated that the volumetric response in the overconsolidated state is almost independent of T and s, leading to a unique value of the parameter

κ^*. Its calibration, based on simulation of a $T = T_0$ and $s = 0$ kPa test (Fig. 4), gives $\kappa^* = 0.002$ as the best approximation.

[Figure 4 about here.]

6.2 Parameters controlling constant s and T response in shear

The critical state friction angle was evaluated using critical state data from the shear experiments on saturated soil, leading to $\varphi_c = 29.5°$. Fig. 5a shows these data, as well the critical state points of all the unsaturated specimens. These results show that the critical state friction angle is independent of temperature and suction. The parameter r controlling the shear stiffness was calibrated using results of drained triaxial shear tests on saturated samples at the reference temperature $T = 25°C$ (Fig. 5). The value of $r = 0.2$ was found to be the most appropriate.

[Figure 5 about here.]

6.3 Parameters controlling the drying-wetting and heating-cooling response

In the model the response due to changes of s and T is treated using different approaches. In the case of heavily overconsolidated soils, predictions due to variable s do not require specification of any parameter since the response is obtained automatically through the influence of $\dot{s}$ on the rate of the effective stress. The response due to heating-cooling cycles in an overconsolidated soil is fully reversible, controlled by the skeletal thermal expansion coefficient α_s. This was calibrated from the results of the heating-cooling experiment on an overconsolidated soil. The coefficient α_s was found to be independent of temperature and suction. The experimental data lead to $\alpha_s = 3.5 \times 10^{-5}$ (see slope of the cooling branch in Fig. 6).

The parameter m influences the distance from the SBS at which the collapsible behaviour due to heating and wetting takes place. It was calibrated using simulations of heating-cooling experiments on an overconsolidated soil (Fig. 6). The values of $m = 2.5$ appeared to best represent the observed behaviour.

[Figure 6 about here.]

The final set of the material parameters is given in Table 1.

[Table 1 about here.]

7 Evaluation of the model predictions

All the simulations presented in the subsequent sections were performed using a single set of material parameters given in Table 1.

7.1 Temperature- and suction-controlled isotropic loading tests

Uchaipchat and Khalili [69] performed a total of 12 isotropic compression tests at different temperatures (25 $^{\circ}C$, 40 $^{\circ}C$ and 60 $^{\circ}C$) and different suctions (0 kPa, 10 kPa, 100 kPa and 300 kPa). Figure 7 shows the model predictions for four representative experiments (temperatures 25 $^{\circ}C$ and 60 $^{\circ}C$ and suctions 0 kPa and 300 kPa), with good agreement between the experimental data and model predictions. It should be noted that Uchaipchat and Khalili [69] observed that the results of the $s = 10$ kPa experiment were almost identical with the results at $s = 0$ kPa. Although this has not been shown in Fig. 7 for clarity, this feature is fully accounted for in the proposed model (suction in the test at $s = 10$ kPa is lower than s_e, therefore the soil is fully saturated and the response coincides with the predictions of the test at $s = 0$ kPa).

[Figure 7 about here.]

7.2 Suction-controlled thermal loading and unloading tests

Volumetric behaviour due to heating and cooling was studied in thermal loading tests at constant suction. Figure 8 shows the results for the experiment on a saturated soil and Fig. 9 presents results of the test at $s = 300$ kPa. The model correctly captures the increasing collapse potential with increasing overconsolidation ratio. The slope of the cooling branch is independent of both suction and overconsolidation ratio and it is controlled solely by the parameter α_s.

[Figure 8 about here.]

[Figure 9 about here.]

7.3 Temperature- and suction-controlled shear tests

Figures 10, 11 and 12 show the results of drained triaxial shear experiments performed at different suction levels, temperatures and overconsolidation ratios. Figures 10 and 11 show

the results of standard drained triaxial tests with constant cell pressure, whereas Fig. 12 shows predictions of "unloading tests", in which the axial stress was kept constant while the cell pressure was reduced. The experimental data demonstrate that, at small cell pressures (higher OCRs), the soil dilates upon shear and shows a pronounced peak in the stress-strain curve, while decreasing OCR increases the contractant response. Increasing temperature reduces the peak strength and induces more contractant response, whereas increasing suction has the reverse effect. All these aspects are captured by the model, with good quantitative agreement between the experimental data and the model predictions. The model also captures the dependency of the soil response on the loading direction, with a greater dilatant response and pronounced peak strength in the unloading tests.

[Figure 10 about here.]

[Figure 11 about here.]

[Figure 12 about here.]

7.4 Constant-water-content thermal loading tests

Finally, the model has been evaluated by means of thermal loading tests under constant water content. Uchaipchat and Khalili [69] performed constant water content experiments on both saturated and unsaturated soil samples. Only the results for the saturated samples are presented here, as calculation of constant water content experiments at unsaturated soils requires definition of the water retention behaviour and complete thermo-hydro-mechanical model including hydraulic hysteresis effects. This will be considered in an upcoming paper.

At saturated conditions, the volume change due to heating is caused by the difference in the thermal expansion coefficients of the solid particles α_s and water α_w:

$$\operatorname{tr} \dot{\boldsymbol{\epsilon}} = \left[\alpha_w n + \alpha_s (1-n)\right] \dot{T} \tag{42}$$

where n is porosity $n = e/(1+e)$. The development of pore pressures is then controlled solely by the constitutive model for the soil mechanical behaviour. The coefficient α_w depends on both temperature and pressure. An empirical expression by Baldi et al. [4] was adopted in the present simulations:

$$\alpha_w = \alpha_0 + (\alpha_1 + \beta_1 T) \ln m u_w + (\alpha_2 + \beta_2 T)(\ln m u_w)^2 \tag{43}$$

where u_w is pore water pressure in kPa and constants are given by $\alpha_0 = 4.505 \times 10^{-4}\ ^\circ C^{-1}$, $\alpha_1 = 9.156 \times 10^{-5}\ ^\circ C^{-1}$, $\beta_1 = -1.2 \times 10^{-6}\ ^\circ C^{-2}$, $\alpha_2 = 6.381 \times 10^{-6}\ ^\circ C^{-1}$, $\beta_2 = -5.766 \times 10^{-8}\ ^\circ C^{-2}$ and $m = 1.5 \times 10^{-6}$ kPa^{-1}.

The experimental results and predictions of pore water pressures due to heating of saturated soils at different initial mean stresses are shown in Figs. 13a and b. The model prediction is in agreement with the experiment results, showing a higher increase in the pore water pressure with an increase in the initial stress. This decrease is controlled by the soil bulk stiffness, which increases with effective stress.

[Figure 13 about here.]

The volumetric response is shown in Figs. 14a and b (void ratio vs. mean effective stress) and c and d (volumetric strain vs. temperature). Also the volumetric response is captured correctly by the model, which shows that the volumetric strain is practically independent of the applied effective stress.

[Figure 14 about here.]

7.5 Temperature-controlled desaturation tests

Figure 15 shows the volume changes imposed by suction increase in desaturation tests at $T = 25^\circ C$ and Fig. 16 gives the equivalent results for $T = 60^\circ C$. The model correctly predicts the general trend of a softer response for specimens with a low overconsolidation ratio (test at $p^{net} = 200$ kPa) and a stiffening of the response once suction reaches the air-entry value. The volume changes during desaturation tests do not depend significantly on temperature. Note that the initial void ratio of the tests at $T = 60^\circ C$ is lower then for the tests at $T = 25^\circ C$, owing to the volume changes prior to the desaturation tests. The soil was first exposed to the target net stresses and then to the target temperatures, which imposed volume decrease due to thermal collapse, especially for the test at low overconsolidation ratio (test at $p^{net} = 200$ kPa).

[Figure 15 about here.]

[Figure 16 about here.]

8 Conclusions

In the paper, we presented a development of a constitutive model for the thermo-mechanical behaviour of unsaturated soils. Since the model is based on the incrementally non-linear hypoplastic model, it allows predictions of the non-linear soil behaviour in the medium- to large-strain range. Its extension to correctly predict the small- to very-small strain behaviour would follow [59, 48], but additional experimental investigation into the influence of temperature on the very small strain behaviour would be needed. The number of model parameters is kept to a minimum. All the parameters have a clear physical interpretation and in the paper we detailed their step-by-step calibration procedures. The model was evaluated with respect to a comprehensive set of experimental data on unsaturated compacted silt given by Uchaipchat and Khalili [69]. Not only can the model correctly predict of the non-linear response of overconsolidated soils, it can also deal with all the primary features of the mechanical behaviour of unsaturated soils under non-isothermal conditions.

9 Acknowledgment

The first author greatly appreciates a Visiting Fellow appointment in the School of Civil and Environmental Engineering of The University of New South Wales, Sydney, where this paper was originated. In addition, financial support by the research grants of the Grant Agency of the Czech Republic GACR 205/08/0732 and MSM 0021620855 is gratefully acknowledged.

References

[1] H. M. Abuel-Naga, D. T. Bergado, A. Bouazza, and M. Pender. Thermomechanical model for saturated clays. *Géotechnique*, 59(3):273–278, 2009.

[2] S. Aversa and A. Evangelista. Thermal expansion of Neapolitan yellow tuff. *Rock Mech. Rock Engng.*, 26(4):281–306, 1993.

[3] J. Bachmann, R. Horton, S. A. Grant, and R. R. van der Ploeg. Temperature dependence of water retention curves for wettable and water-repellent soils. *Soil Science Society of America Journal*, 66:44–52, 2002.

[4] G. Baldi, T. Hueckel, and R. Pellegrini. Thermal volume changes of the mineral - water system in low-porosity clay soils. *Canadian Geotechnical Journal*, 25:807–825, 1988.

[5] A. W. Bishop. The principle of effective stress. *Teknisk Ukeblad*, 106(39):859–863, 1959.

[6] G. Bolzon and A. Schrefler. Thermal effects in partially saturated soils: a constitutive model. *International Journal for Numerical and Analytical Methods in Geomechanics*, 29:861–877, 2005.

[7] A. Burghignoli, A. Desideri, and S. Miliziano. A laboratory study on the thermomechanical behaviour of clayey soils. *Canadian Geotechnical Journal*, 37:764–780, 2000.

[8] R. Butterfield. A natural compression law for soils. *Géotechnique*, 29(4):469–480, 1979.

[9] R. G. Campanella and J. K. Mitchell. Influence of temperature variations on soil behaviour. *Journal of the Soil Mechanics and Foundations Division ASCE*, 94(3):709–734, 1968.

[10] C. Cekerevac and L. Laloui. Experimental study of thermal effects on the mechanical behaviour of a clay. *International Journal for Numerical and Analytical Methods in Geomechanics*, 28:209–228, 2004.

[11] Y. J. Cui, N. Sultan, and P. Delage. A thermomechanical model for saturated clays. *Canadian Geotechnical Journal*, 37:607–620, 2000.

[12] D. De Bruyn and J.-F. Thimus. The influence of temperature on mechanical characteristics of Boom clay: The results of an initial laboratory programme. *Engineering Geology*, 41:117–126, 1996.

[13] C. Del Olmo, V. Fioravante, F. Gera, T. Hueckel, J. C. Mayor, and R. Pellegrini. Thermomechanical properties of deep argillaceous formations. *Engineering Geology*, 41:87–101, 1996.

[14] K. R. Demars and R. D. Charles. Soil volume changes induced by temperature cycling. *Canadian Geotechnical Journal*, 19:188–194, 1982.

[15] B. François and L. Laloui. ACMEG-TS: A constitutive model for unsaturated soils under non-isothermal conditions. *International Journal for Numerical and Analytical Methods in Geomechanics*, 32:1955–1988, 2008.

[16] M. D. Fredlund, G. W. Wilson, and D. G. Fredlund. Use of the grain-size distribution for estimation of the soil-water characteristic curve. *Canadian Geotechnical Journal*, 39:1103–1117, 2002.

[17] D. Gallipoli, A. Gens, R. Sharma, and J. Vaunat. An elasto-plastic model for unsaturated soil incorporating the effects of suction and degree of saturation on mechanical behaviour. *Géotechnique*, 53(1):123–135, 2003.

[18] J. Graham, N. Tanaka, T. Crilly, and M. Alfaro. Modified Cam-Clay modelling of temperature effects in clays. *Canadian Geotechnical Journal*, 38:608–621, 2001.

[19] S. A. Grant. Extension of temperature effects model for capillary pressure saturation relations. *Water Resources Research*, 39(1):1003, 2003.

[20] S. A. Grant and A. Salehzadeh. Calculation of temperature effects on wetting coefficients of porous solids and their capillary pressure functions. *Water Resources Research*, 32(2):261–270, 1996.

[21] G. Gudehus. A comprehensive constitutive equation for granular materials. *Soils and Foundations*, 36(1):1–12, 1996.

[22] G. Gudehus, A. Amorosi, A. Gens, I. Herle, D. Kolymbas, D. Mašín, D. Muir Wood, R. Nova, A. Niemunis, M. Pastor, C. Tamagnini, and G. Viggiani. The soilmodels.info project. *International Journal for Numerical and Analytical Methods in Geomechanics*, 32(12):1571–1572, 2008.

[23] G. Gudehus and D. Mašín. Graphical representation of constitutive equations. *Géotechnique*, 52(2):147–151, 2009.

[24] V. Hájek, D. Mašín, and J. Boháč. Capability of constitutive models to simulate soils with different OCR using a single set of parameters. *Computers and Geotechnics*, 36(4):655–664, 2009.

[25] I. Herle and D. Kolymbas. Hypoplasticity for soils with low friction angles. *Computers and Geotechnics*, 31(5):365–373, 2004.

[26] G. T. Houlsby. The work input to an unsaturated granular material. *Géotechnique*, 47(1):193–196, 1997.

[27] S. L. Houston, W. N. Houston, and N. D. Williams. Thermo-mechanical behaviour of seafloor sediments. *Journal of Geotechnical Engineering ASCE*, 111(11):1249–1263, 1985.

[28] T. Hueckel and G. Baldi. Thermoplasticity of saturated clays: Experimental constitutive study. *Journal of Geotechnical Engineering ASCE*, 116(12):1778–1796, 1990.

[29] T. Hueckel and M. Borsetto. Thermoplasticity of saturated soils and shales: Constitutive equations. *Journal of Geotechnical Engineering ASCE*, 116(12):1765–1777, 1990.

[30] T. Hueckel, B. François, and L. Laloui. Explaining thermal failure in saturated soils. *Géotechnique*, 59(3):197–212, 2009.

[31] T. Hueckel, R. Pellegrini, and C. Del Olmo. A constitutive study of thermo-elasto-plasticity of deep carbonatic clays. *International Journal for Numerical and Analytical Methods in Geomechanics*, 22:549–574, 1998.

[32] J. E. B. Jennings and J. B. Burland. Limitations to the use of effective stresses in saturated soils. *Géotechnique*, 12(2):125–144, 1962.

[33] N. Khalili, F. Geiser, and G. E. Blight. Effective stress in unsaturated soils: review with new evidence. *International Journal of Geomechanics*, 4(2):115–126, 2004.

[34] N. Khalili, M. A. Habte, and S. Zargarbashi. A fully coupled flow-deformation model for cyclic analysis of unsaturated soils including hydraulic and mechanical hystereses. *Computers and Geotechnics*, 35(6):872–889, 2008.

[35] N. Khalili and M. H. Khabbaz. A unique relationship for χ for the determination of the shear strength of unsaturated soils. *Géotechnique*, 48(2):1–7, 1998.

[36] N. Khalili, A. Uchaipichat, and A. A. Javadi. Skeletal thermal expansion coefficient and thermo-hydro-mechanical constitutive relations for saturated porous media. *Mechanics of Materials (under review)*, 2010.

[37] N. Khalili and S. Zargarbashi. Influence of hydraulic hysteresis on effective stress in unsaturated soils. *Géotechnique (in press)*, 2010.

[38] D. Kolymbas and I. Herle. Shear and objective stress rates in hypoplasticity. *International Journal for Numerical and Analytical Methods in Geomechanics*, 27:733–744, 2003.

[39] P. Kuntiwattanakul, I. Towhata, K. Ohishi, and I. Seko. Temperature effects on undrained shear characteristics of clay. *Soils and Foundations*, 35(1):147–162, 1995.

[40] L. Laloui and C. Cekerevac. Thermo-plasticity of clays: An isotropic yield mechanism. *Computers and Geotechnics*, 30:649–660, 2003.

[41] L. Laloui and C. Cekerevac. Non-isothermal plasticity model for cyclic behaviour of soils. *International Journal for Numerical and Analytical Methods in Geomechanics*, 32:437–460, 2008.

[42] L. Laloui and C. Cekerevac. Numerical simulation of the non-isothermal mechanical behaviour of soils. *Computers and Geotechnics*, 35:729–745, 2008.

[43] X. S. Li. Effective stress in unsaturated soil: a microstructural analysis. *Géotechnique*, 53, 2003.

[44] B. E. Lingau, J. Graham, and N. Tanaka. Isothermal modelling of sand-bentonite mixtures at elevated temperatures. *Canadian Geotechnical Journal*, 32:78–88, 1995.

[45] B. E. Lingau, J. Graham, D. Yarechewski, N. Tanaka, and M. N. Gray. Effects of temperature on strength and compressibility of sand-bentonite buffer. *Engineering Geology*, 41:103–115, 1996.

[46] B. Loret and N. Khalili. A three-phase model for unsaturated soils. *International Journal for Numerical and Analytical Methods in Geomechanics*, 24:893–927, 2000.

[47] H. Matsuoka and T. Nakai. Stress–deformation and strength characteristics of soil under three different principal stresses. In *Proc. Japanese Soc. of Civil Engineers*, volume 232, pages 59–70, 1974.

[48] D. Mašín. A hypoplastic constitutive model for clays. *International Journal for Numerical and Analytical Methods in Geomechanics*, 29(4):311–336, 2005.

[49] D. Mašín. A hypoplastic constitutive model for clays with meta-stable structure. *Canadian Geotechnical Journal*, 44(3):363–375, 2007.

[50] D. Mašín. 3D modelling of a NATM tunnel in high K_0 clay using two different constitutive models. *Journal of Geotechnical and Geoenvironmental Engineering ASCE*, 135(9):1326–1335, 2009.

[51] D. Mašín. Comparison of predictive capabilities of selected elasto-plastic and hypoplastic models for structured clays. *Soils and Foundations*, 49(3):381–390, 2009.

[52] D. Mašín. Predicting the dependency of a degree of saturation on void ratio and suction using effective stress principle for unsaturated soils. *International Journal for Numerical and Analytical Methods in Geomechanics*, 34:73–90, 2010.

[53] D. Mašín and I. Herle. State boundary surface of a hypoplastic model for clays. *Computers and Geotechnics*, 32(6):400–410, 2005.

[54] D. Mašín and N. Khalili. A hypoplastic model for mechanical response of unsaturated soils. *International Journal for Numerical and Analytical Methods in Geomechanics*, 32(15):1903–1926, 2008.

[55] D. Mašín, C. Tamagnini, G. Viggiani, and D. Costanzo. Directional response of a reconstituted fine grained soil. Part II: performance of different constitutive models. *International Journal for Numerical and Analytical Methods in Geomechanics*, 30(13):1303–1336, 2006.

[56] H. Modaressi and L. Laloui. A thermo-viscoplastic constitutive model for clays. *International Journal for Numerical and Analytical Methods in Geomechanics*, 21:313–335, 1997.

[57] D. Muir Wood and A. Gajo. Hierarchical critical state models. In J. A. Yamamuro and V. N. Kaliakin, editors, *Soil Constitutive Models, Evaluation, Selection, and Calibration (Geotechnical Special Publication No. 128)*, pages 459–482. ASCE, 2005.

[58] A. Niemunis. *Extended Hypoplastic Models for Soils*. Habilitation thesis, Ruhr-University, Bochum, 2002.

[59] A. Niemunis and I. Herle. Hypoplastic model for cohesionless soils with elastic strain range. *Mechanics of Cohesive-Frictional Materials*, 2:279–299, 1997.

[60] E. Romero, A. Gens, and A. Lloret. Temperature effects on the hydraulic behaviour of an unsaturated clay. *Geotechnical and Geological Engineering*, 19:311–332, 2001.

[61] E. Romero, A. Gens, and A. Lloret. Suction effects on a compacted clay under non-isothermal conditions. *Géotechnique*, 53(1):65–81, 2003.

[62] K. H. Roscoe and J. B. Burland. On the generalised stress-strain behaviour of wet clay. In J. Heyman and F. A. Leckie, editors, *Engineering Plasticity*, pages 535–609. Cambridge: Cambridge University Press, 1968.

[63] A. N. Schofield and C. P. Wroth. *Critical State Soil Mechanics*. McGraw-Hill Book Co., London, 1968.

[64] H. Y. She and B. E. Sleep. The effect of temperature on capillary pressure-saturation relationships for air-water and perchlorethylene-water systems. *Water Resources Research*, 34(10):2587–2597, 1998.

[65] N. Sultan, P. Delage, and Y. J. Cui. Temperature effects on the volume change behaviour of Boom clay. *Engineering Geology*, 64:135–145, 2002.

[66] C. Tamagnini, G. Viggiani, and R. Chambon. A review of two different approaches to hypoplasticity. In D. Kolymbas, editor, *Constitutive Modelling of Granular Materials*, pages 107–144. Springer, 2000.

[67] N. Tanaka, J. Graham, and T. Crilly. Stress-strain behaviour of reconstituted illitic clay at different temperatures. *Engineering Geology*, 47:339–350, 1997.

[68] I. Towhata, P. Kuntiwattanakul, I. Seko, and K. Ohishi. Volume change of clays induced by heating as observed in consolidation tests. *Soils and Foundations*, 33(4):170–183, 1993.

[69] A. Uchaipchat and N. Khalili. Experimental investigation of thermo-hydro-mechanical behaviour of an unsaturated silt. *Géotechnique*, 59(4):339–353, 2009.

[70] P. A. von Wolffersdorff. A hypoplastic relation for granular materials with a predefined limit state surface. *Mechanics of Cohesive-Frictional Materials*, 1:251–271, 1996.

[71] B. Wiebe, J. Graham, G. X. Tang, and D. Dixon. Influence of pressure, saturation, and temperature on the behaviour of unsaturated sand-bentonite. *Canadian Geotechnical Journal*, 35:194–205, 1998.

[72] W. Wu, X. Li, R. Charlier, and F. Collin. A thermo-hydro-mechanical constitutive model and its numerical modelling for unsaturated soils. *Computers and Geotechnics*, 31:155–167, 2004.

Appendix 1

The mathematical formulation of the proposed hypoplastic model is summarised briefly in the following. The rate formulation of the model reads

$$\mathring{\boldsymbol{\sigma}} = f_s \left[\boldsymbol{\mathcal{L}} : (\dot{\boldsymbol{\epsilon}} - \dot{\boldsymbol{\epsilon}}^{TE}) + f_d \mathbf{N} \| \dot{\boldsymbol{\epsilon}} - \dot{\boldsymbol{\epsilon}}^{TE} \| \right] + f_u \left(\mathbf{H}_s + \mathbf{H}_T \right) \tag{44}$$

$\boldsymbol{\sigma}$ and $\mathring{\boldsymbol{\sigma}}$ are the effective stress and the objective effective stress rate tensors respectively, defined by

$$\boldsymbol{\sigma} = \boldsymbol{\sigma}^{net} - \chi s \mathbf{1} \qquad \mathring{\boldsymbol{\sigma}} = \mathring{\boldsymbol{\sigma}}^{net} - \psi \dot{s} \mathbf{1} \tag{45}$$

where $\boldsymbol{\sigma}_{net} = \boldsymbol{\sigma}^{tot} + u_a \mathbf{1}$ is a net stress, with $\boldsymbol{\sigma}^{tot}$ being a total stress, u_a the pore air pressure and u_w the pore water pressure. s is the matric suction $s = u_a - u_w$. The effective stress factor χ is defined by [35]

$$\chi = \begin{cases} 1 & \text{for} \quad s < s_e \\ \left(\dfrac{s_e}{s} \right)^{\gamma} & \text{for} \quad s \geq s_e \end{cases} \tag{46}$$

where s_e is a model parameter and $\gamma = 0.55$. $\psi = (1 - \gamma)\chi$ for $s \geq s_e$ and $\psi = 1$ otherwise.

$\dot{\boldsymbol{\epsilon}}$ is the Euler stretching tensor and $\dot{\boldsymbol{\epsilon}}^{TE}$ is the reversible component of the thermally-induced strain rate:

$$\dot{\boldsymbol{\epsilon}}^{TE} = \frac{\mathbf{1}}{3}\alpha_s \dot{T} \tag{47}$$

where T is temperature and α_s is a model parameter.

The fourth-order tensor $\boldsymbol{\mathcal{L}}$ is a hypoelastic tensor given by

$$\boldsymbol{\mathcal{L}} = 3\left(c_1 \boldsymbol{\mathcal{I}} + c_2 a^2 \hat{\boldsymbol{\sigma}} \otimes \hat{\boldsymbol{\sigma}}\right) \tag{48}$$

with $\hat{\boldsymbol{\sigma}} = \boldsymbol{\sigma}/\operatorname{tr}\boldsymbol{\sigma}$. The two scalar factors c_1 and c_2 were introduced in [25] and modified in [48]:

$$c_1 = \frac{2\left(3 + a^2 - 2^{\alpha} a\sqrt{3}\right)}{9r} \qquad\qquad c_2 = 1 + (1 - c_1)\frac{3}{a^2} \tag{49}$$

where r is a model parameter and the scalars a and α are functions of the material parameters φ_c, λ^* and κ^*

$$a = \frac{\sqrt{3}\,(3 - \sin\varphi_c)}{2\sqrt{2}\sin\varphi_c} \qquad\qquad \alpha = \frac{1}{\ln 2}\ln\left[\frac{\lambda^* - \kappa^*}{\lambda^* + \kappa^*}\left(\frac{3 + a^2}{a\sqrt{3}}\right)\right] \tag{50}$$

The second-order tensor $\mathbf{N}$ is given by [58]

$$\mathbf{N} = \boldsymbol{\mathcal{L}} : \left(Y \frac{\mathbf{m}}{\|\mathbf{m}\|}\right) \tag{51}$$

where the quantity Y determines the shape of the critical state locus in the stress space such that for $Y = 1$ it coincides with the Matsuoka and Nakai [47] limit stress condition.

$$Y = \left(\frac{\sqrt{3}a}{3 + a^2} - 1\right)\frac{(I_1 I_2 + 9I_3)\left(1 - \sin^2\varphi_c\right)}{8I_3 \sin^2\varphi_c} + \frac{\sqrt{3}a}{3 + a^2} \tag{52}$$

with the stress invariants

$$I_1 = \operatorname{tr}(\boldsymbol{\sigma}) \qquad\qquad I_2 = \frac{1}{2}\left[\boldsymbol{\sigma} : \boldsymbol{\sigma} - (I_1)^2\right] \qquad\qquad I_3 = \det(\boldsymbol{\sigma})$$

$\det(\boldsymbol{\sigma})$ is the determinant of $\boldsymbol{\sigma}$. The second-order tensor $\mathbf{m}$ is calculated by

$$\mathbf{m} = -\frac{a}{F}\left[\hat{\boldsymbol{\sigma}} + \operatorname{dev}\hat{\boldsymbol{\sigma}} - \frac{\hat{\boldsymbol{\sigma}}}{3}\left(\frac{6\hat{\boldsymbol{\sigma}} : \hat{\boldsymbol{\sigma}} - 1}{(F/a)^2 + \hat{\boldsymbol{\sigma}} : \hat{\boldsymbol{\sigma}}}\right)\right] \tag{53}$$

with the factor F

$$F = \sqrt{\frac{1}{8}\tan^2\psi + \frac{2-\tan^2\psi}{2+\sqrt{2}\tan\psi\cos 3\theta}} - \frac{1}{2\sqrt{2}}\tan\psi \tag{54}$$

where

$$\tan\psi = \sqrt{3}\,\|\mathrm{dev}\,\hat{\boldsymbol{\sigma}}\| \qquad\qquad \cos 3\theta = -\sqrt{6}\frac{\mathrm{tr}\,(\mathrm{dev}\,\hat{\boldsymbol{\sigma}}\cdot\mathrm{dev}\,\hat{\boldsymbol{\sigma}}\cdot\mathrm{dev}\,\hat{\boldsymbol{\sigma}})}{[\mathrm{dev}\,\hat{\boldsymbol{\sigma}}:\mathrm{dev}\,\hat{\boldsymbol{\sigma}}]^{3/2}} \tag{55}$$

The *barotropy* factor f_s introduces the influence of the mean stress level

$$f_s = \frac{3p}{\lambda^*(s,T)}\left(3 + a^2 - 2^\alpha a\sqrt{3}\right)^{-1} \tag{56}$$

and the *pyknotropy* factor f_d incorporates the influence of the overconsolidation ratio.

$$f_d = \left(\frac{2p}{p_e}\right)^\alpha \qquad\qquad p_e = p_r \exp\left[\frac{N(s,T) - \ln(1+e)}{\lambda^*(s,T)}\right] \tag{57}$$

where $p_r = 1$ kPa is the reference stress. Values of $N(s,T)$ and $\lambda^*(s,T)$ are represented by

$$N(s,T) = N + n_s\left\langle \ln\frac{s}{s_e}\right\rangle + n_T \ln\left(\frac{T}{T_0}\right) \qquad \lambda^*(s,T) = \lambda^* + l_s\left\langle \ln\frac{s}{s_e}\right\rangle + l_T\ln\left(\frac{T}{T_0}\right) \tag{58}$$

N, λ^*, n_s, l_s, n_T, l_T and T_0 are model parameters.

The tensorial terms $\mathbf{H}_s$ and $\mathbf{H}_T$ from Eq. (44) read

$$\mathbf{H}_s = -c_i\frac{\boldsymbol{\sigma}}{s\lambda^*(s,T)}\left[n_s - l_s\ln\frac{p_e}{p_r}\right]\langle -\dot{s}\rangle \tag{59}$$

for $s > s_e$ and $\mathbf{H}_s = \mathbf{0}$ otherwise, and

$$\mathbf{H}_T = c_i\frac{\boldsymbol{\sigma}}{T\lambda^*(s,T)}\left[n_T - l_T\ln\frac{p_e}{p_r}\right]\langle \dot{T}\rangle \tag{60}$$

with

$$c_i = \frac{3 + a^2 - f_d a\sqrt{3}}{3 + a^2 - f_d^{SBS} a\sqrt{3}} \tag{61}$$

f_d^{SBS} is the value of the pyknotropy factor f_d for states at the SBS, defined as [53]

$$f_d^{SBS} = \|f_s\boldsymbol{\mathcal{A}}^{-1} : \mathbf{N}\|^{-1} \tag{62}$$

where the fourth-order tensor $\boldsymbol{\mathcal{A}}$ is expressed by

$$\boldsymbol{\mathcal{A}} = f_s \boldsymbol{\mathcal{L}} - \frac{1}{\lambda^*(s,T)} \boldsymbol{\sigma} \otimes \mathbf{1} \tag{63}$$

The factor controlling the collapsible behaviour f_u reads

$$f_u = \left(\frac{f_d}{f_d^{SBS}} \right)^{m/\alpha} \tag{64}$$

with m being a model parameter.

Finally, evolution of the state variable e (void ratio) is governed by

$$\dot{e} = (1+e)\,\mathrm{tr}\,(\dot{\boldsymbol{\epsilon}} - \dot{\boldsymbol{\epsilon}}^{TE}) \tag{65}$$

The model requires 13 parameters: φ_c, λ^*, κ^*, N, r, n_s, l_s, n_T, l_T, α_s, m, s_e and T_0.

Appendix 2

This appendix shows the derivation of the isotropic formulation of Eq. (27). Eq (27) reads

$$-c_i \mathbf{H}_T = f_s \left[\boldsymbol{\mathcal{L}} : (\dot{\boldsymbol{\epsilon}} - \dot{\boldsymbol{\epsilon}}^{TE}) + f_d \mathbf{N} \| \dot{\boldsymbol{\epsilon}} - \dot{\boldsymbol{\epsilon}}^{TE} \| \right] \tag{66}$$

At isotropic conditions, we have (from (8))

$$\dot{\boldsymbol{\epsilon}} - \dot{\boldsymbol{\epsilon}}^{TE} = \mathbf{1} \frac{\dot{e}}{3(1+e)} \tag{67}$$

Applying operation $-\,\mathrm{tr}\,(x)/3$ on Eq. (66), we get

$$\frac{c_i\,\mathrm{tr}\,\mathbf{H}_T}{3} = -\frac{f_s}{3(1+e)} \left[\frac{\mathrm{tr}(\boldsymbol{\mathcal{L}} : \mathbf{1})}{3} \dot{e} + f_d \frac{\mathrm{tr}(\mathbf{N})}{3} \sqrt{3} |\dot{e}| \right] \tag{68}$$

In evaluation of the factor c_i, we are interested in the thermal collapse, thus $\dot{e} < 0$. Definition of variables $\boldsymbol{\mathcal{L}}$ and $\mathbf{N}$ is in Appendix 1 (Eqs. (48) and (51)). It follows from their formulations that at the isotropic state

$$\frac{\mathrm{tr}(\boldsymbol{\mathcal{L}} : \mathbf{1})}{3} = 3 + a^2 \qquad \text{and} \qquad \frac{\mathrm{tr}(\mathbf{N})}{3} = a \tag{69}$$

a is defined in Eq. (50). For more details on (69), see [48]. Combination of (69) with (68) with the condition $\dot{e} < 0$ leads us to

$$c_i \frac{\mathrm{tr}\,\mathbf{H}_T}{3} = -\frac{f_s}{3}\left[3 + a^2 - f_d a\sqrt{3}\right]\frac{\dot{e}}{1+e} \tag{70}$$

Finally, formulation of the *barotropy* factor f_s (Eq. (56)) may be included into (70), giving us

$$c_i \frac{\mathrm{tr}(\mathbf{H}_T)}{3} = -\frac{p}{\lambda^*}\left[\frac{3 + a^2 - f_d a\sqrt{3}}{3 + a^2 - 2^\alpha a\sqrt{3}}\right]\frac{\dot{e}}{1+e} \tag{71}$$

The factor α is defined in (50).

List of Figures

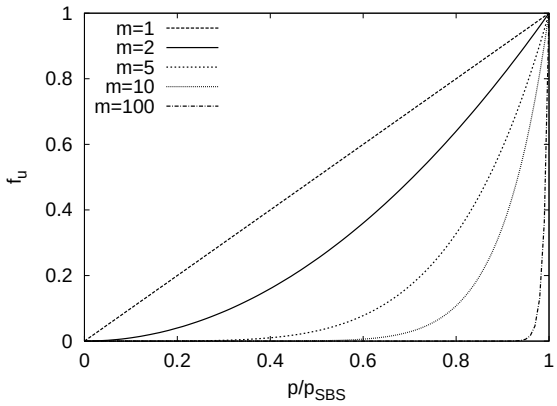

Figure 1: The influence of the parameter m on the value of the factor f_u (from [54]).

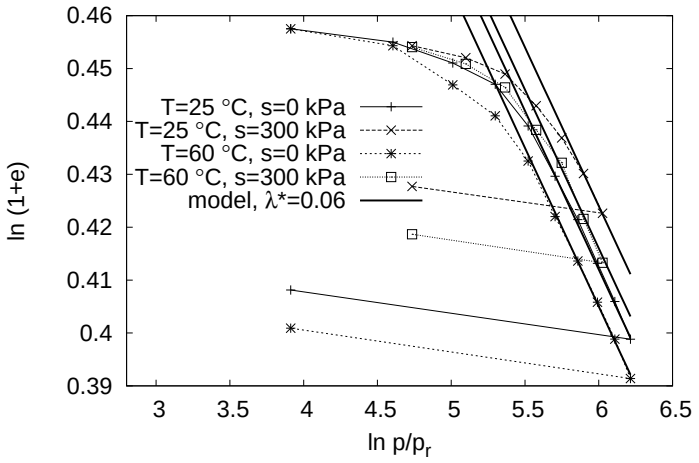

Figure 2: Results of the isotropic compression tests at different suctions and temperatures plotted in the effective stress space and model representation of NCLs.

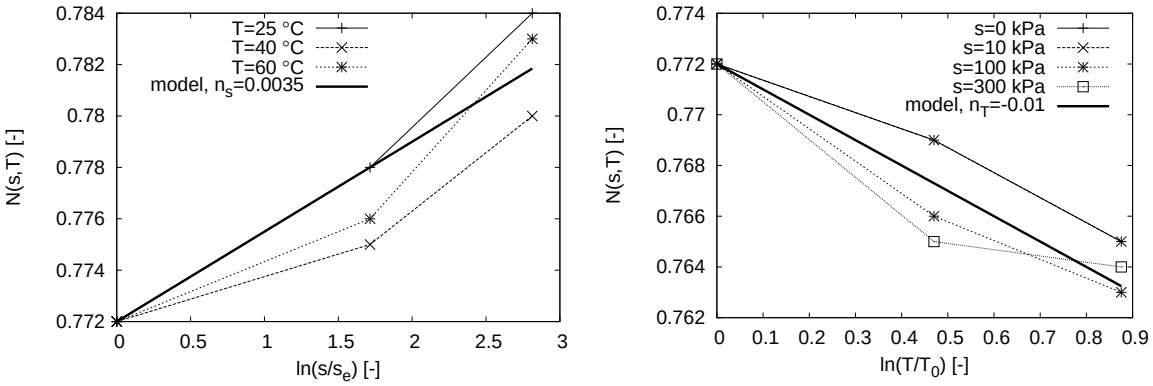

(a) (b)

Figure 3: Calibration of parameters n_s (a) and n_T (b). In (b), curves for $s = 0$ kPa and $s = 10$ kPa are overlapping, as $s < s_e$.

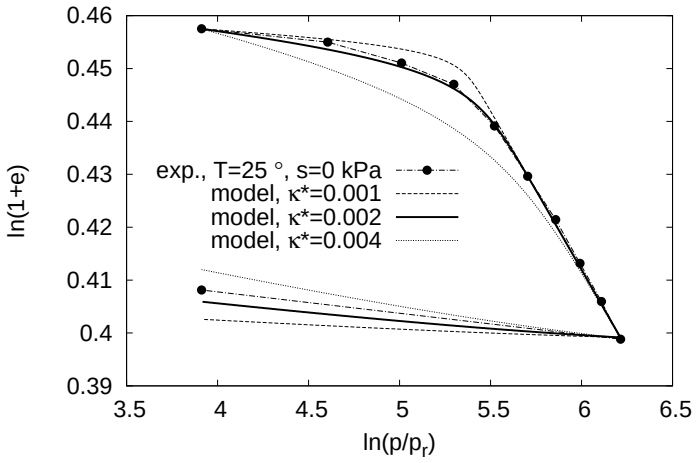

Figure 4: Calibration of the parameter κ^* by means of simulations of a $T = 25\ ^\circ C$ and $s = 0$ kPa isotropic loading and unloading experiment.

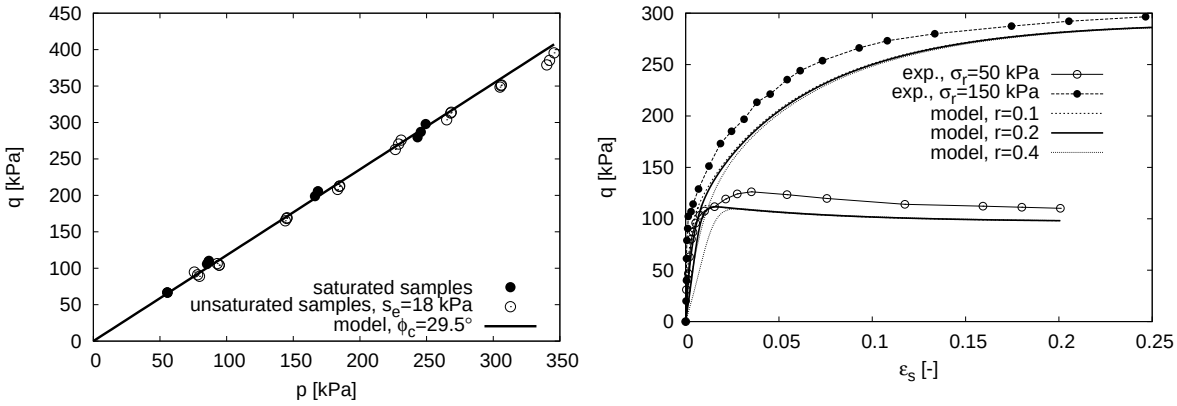

(a) (b)

Figure 5: Calibration of the parameter critical state friction angle (a) and the parameter r (b).

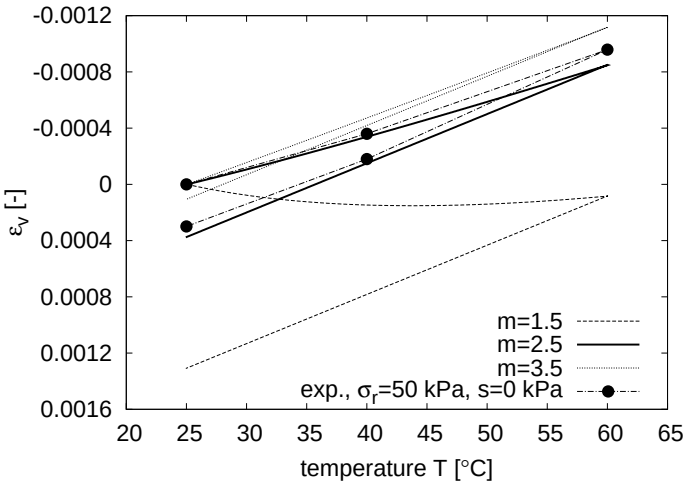

Figure 6: Calibration of the parameter m using heating-cooling experiments on an unsaturated soil at different stress levels (different overconsolidation ratios).

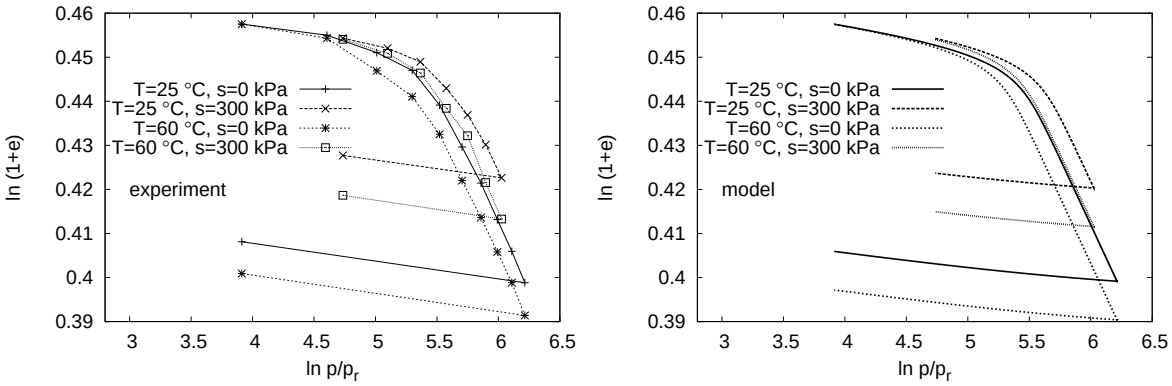

(a) (b)

Figure 7: Comparison of experimental data (a) and simulations (b) of representative isotropic compression experiments at different suctions and temperatures.

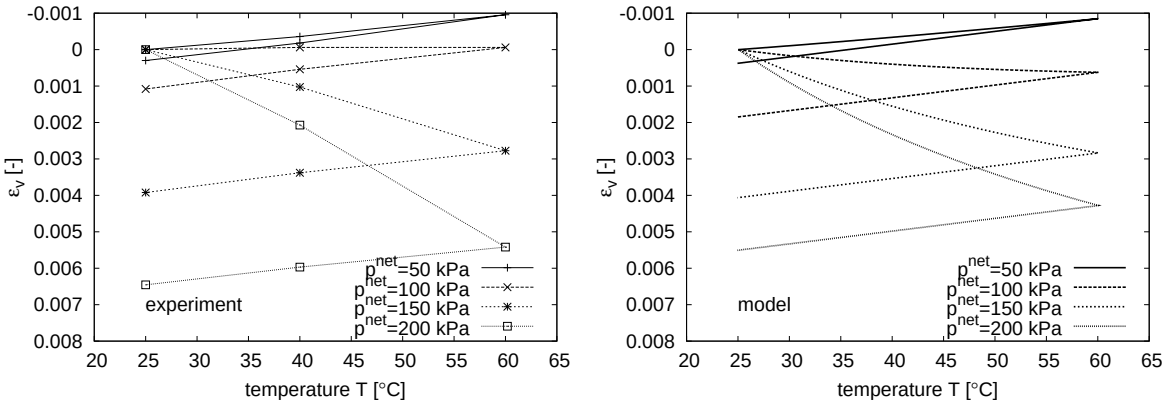

(a) (b)

Figure 8: Volumetric change due to heating-cooling cycle in experiments at $s = 0$ kPa and different stress levels. (a) experiment, (b) model.

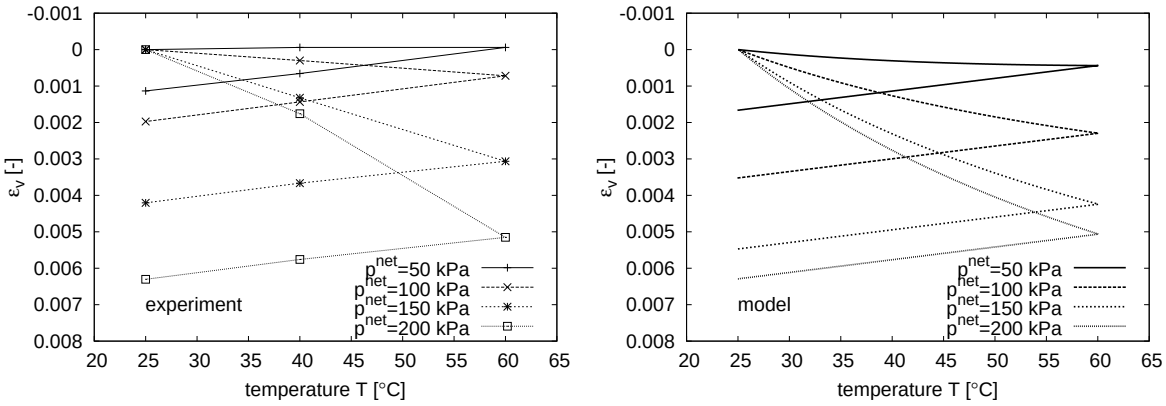

(a) (b)

Figure 9: Volumetric change due to heating-cooling cycle in experiments at $s = 300$ kPa and different stress levels. (a) experiment, (b) model.

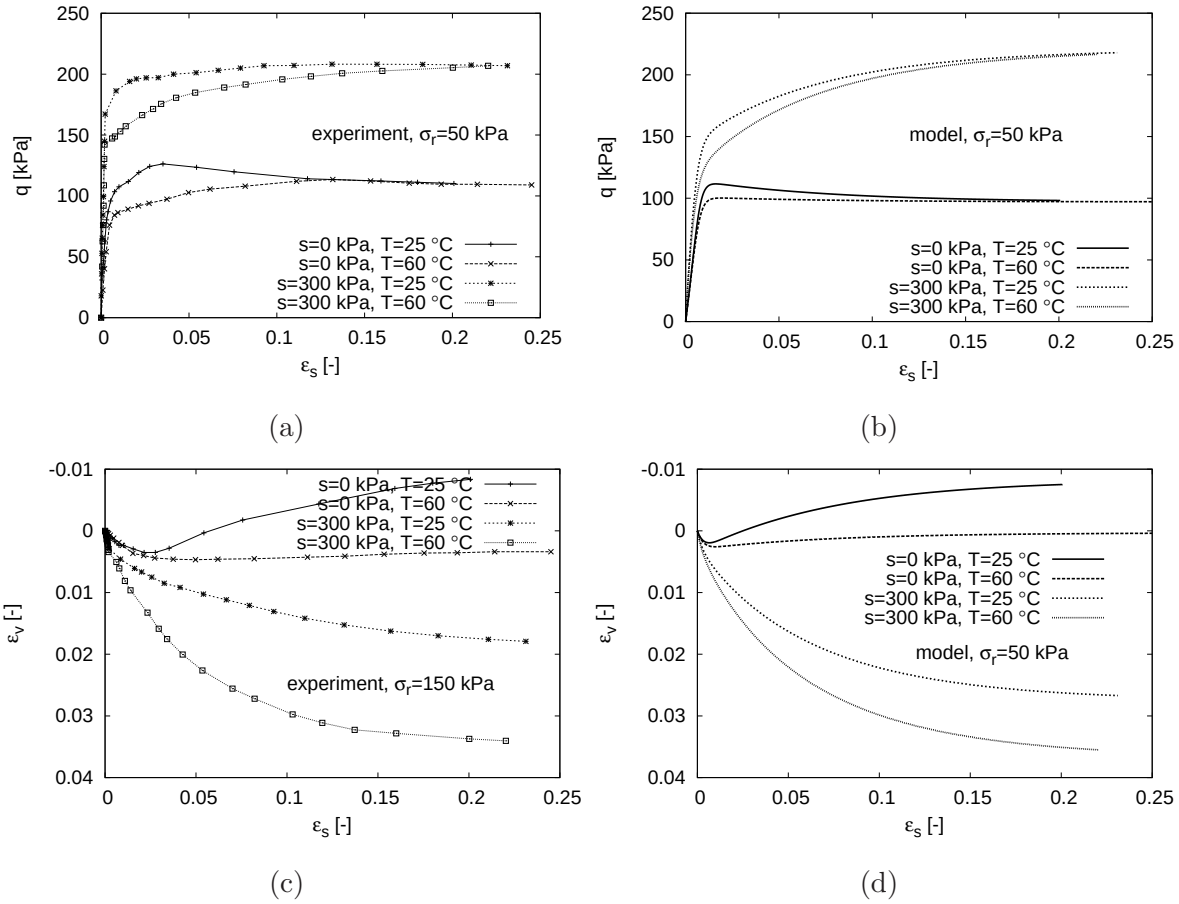

Figure 10: Experimental results (a,c) and predictions (b,d) of temperature- and suction-controlled shear tests at $\sigma_r = 50$ kPa.

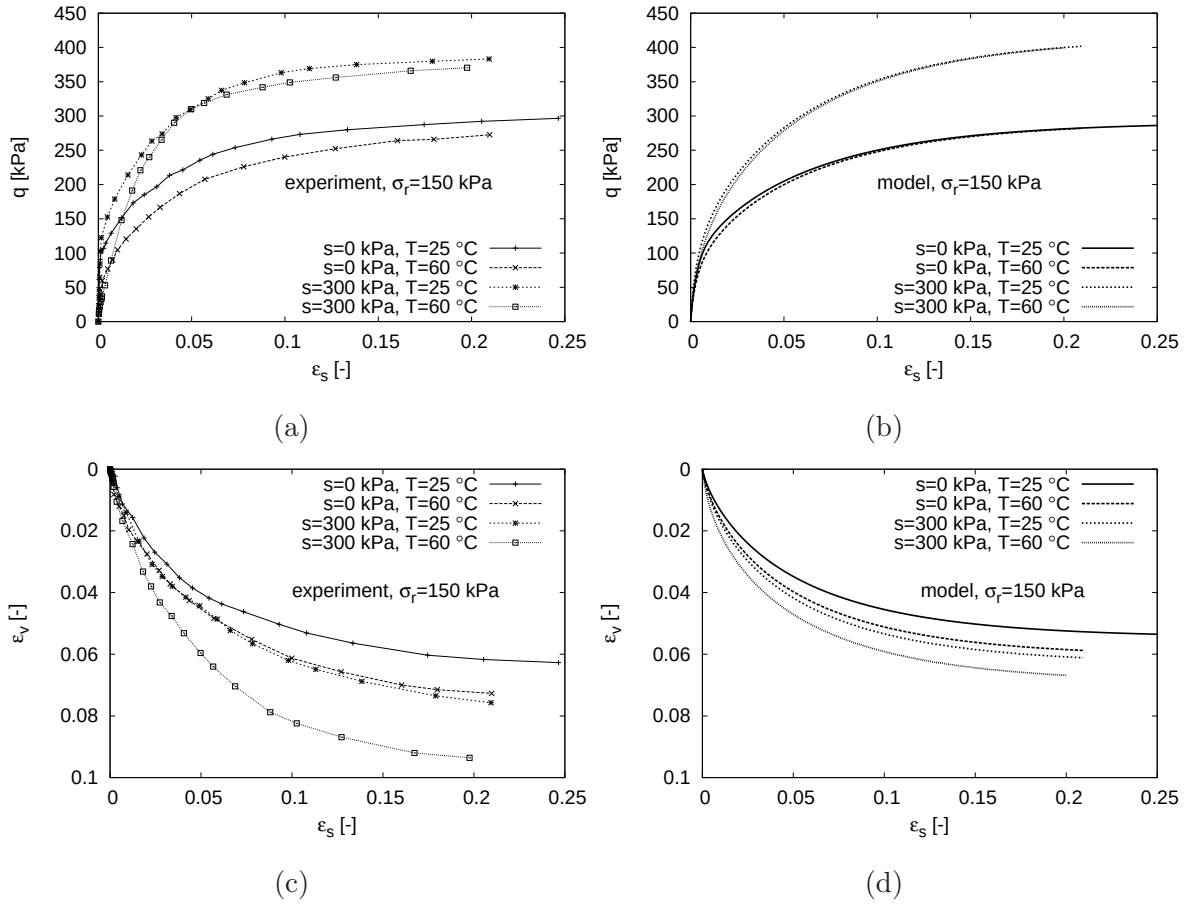

Figure 11: Experimental results (a,c) and predictions (b,d) of temperature- and suction-controlled shear tests at $\sigma_r = 150$ kPa.

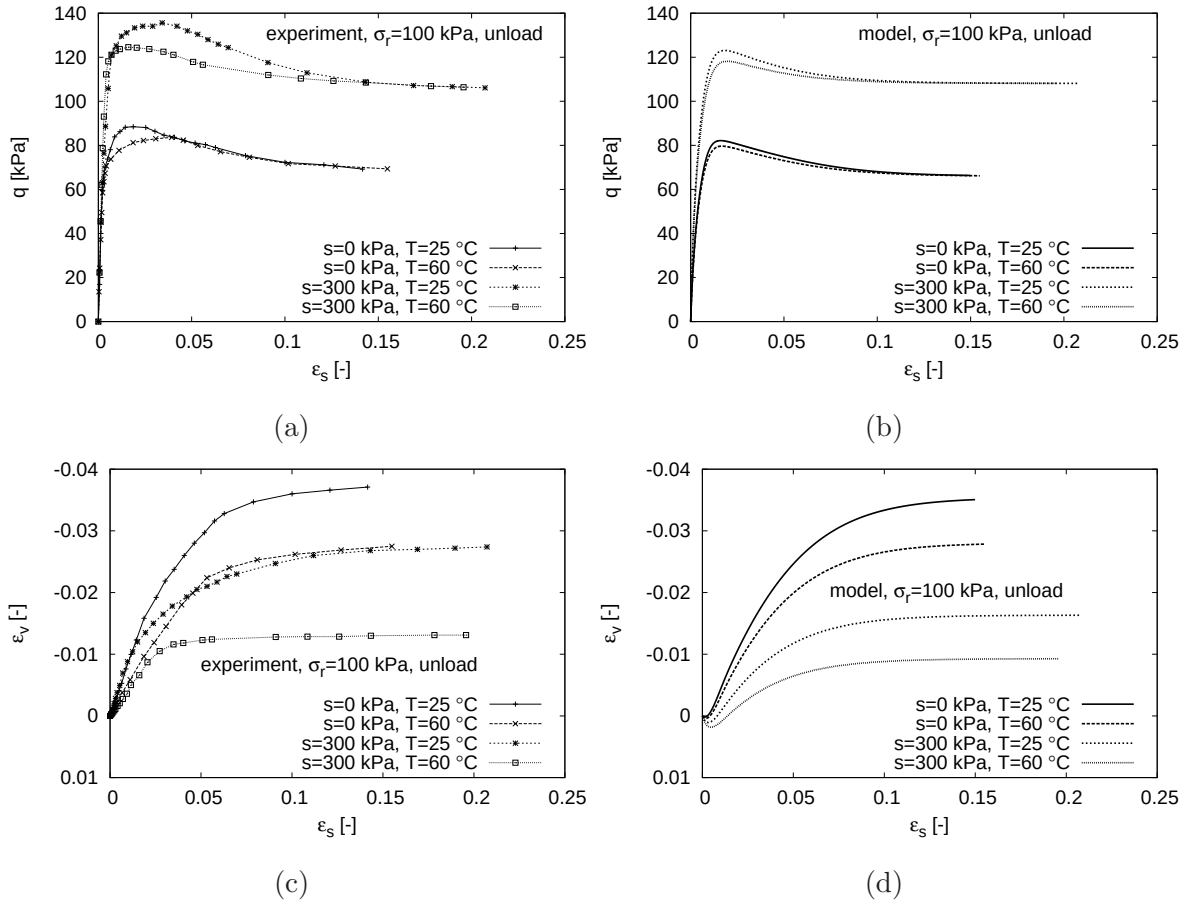

Figure 12: Experimental results (a,c) and predictions (b,d) of temperature- and suction-controlled shear tests at $\sigma_r = 100$ kPa, "unloading path".

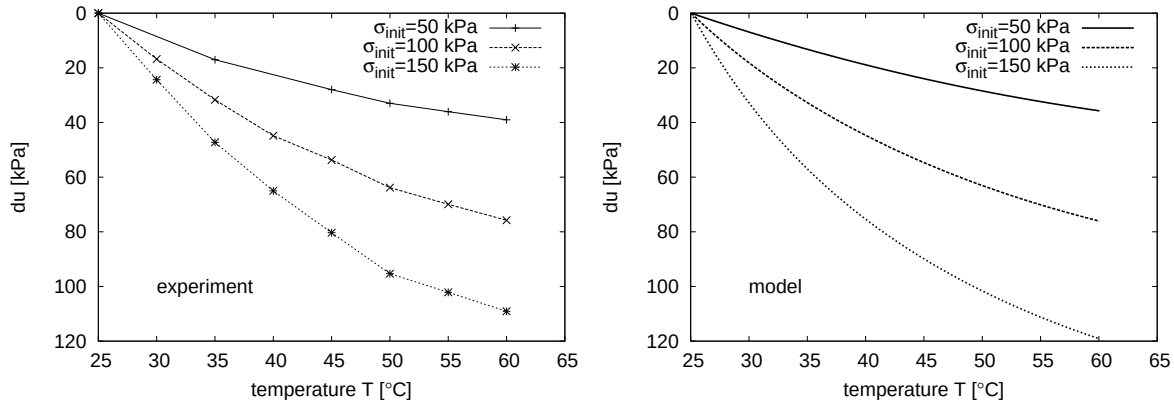

(a) (b)

Figure 13: Experimental results (a) and model predictions (b) of pore pressure change during constant-water-content (undrained) heating experiments on saturated soil at different effective stresses (OCRs).

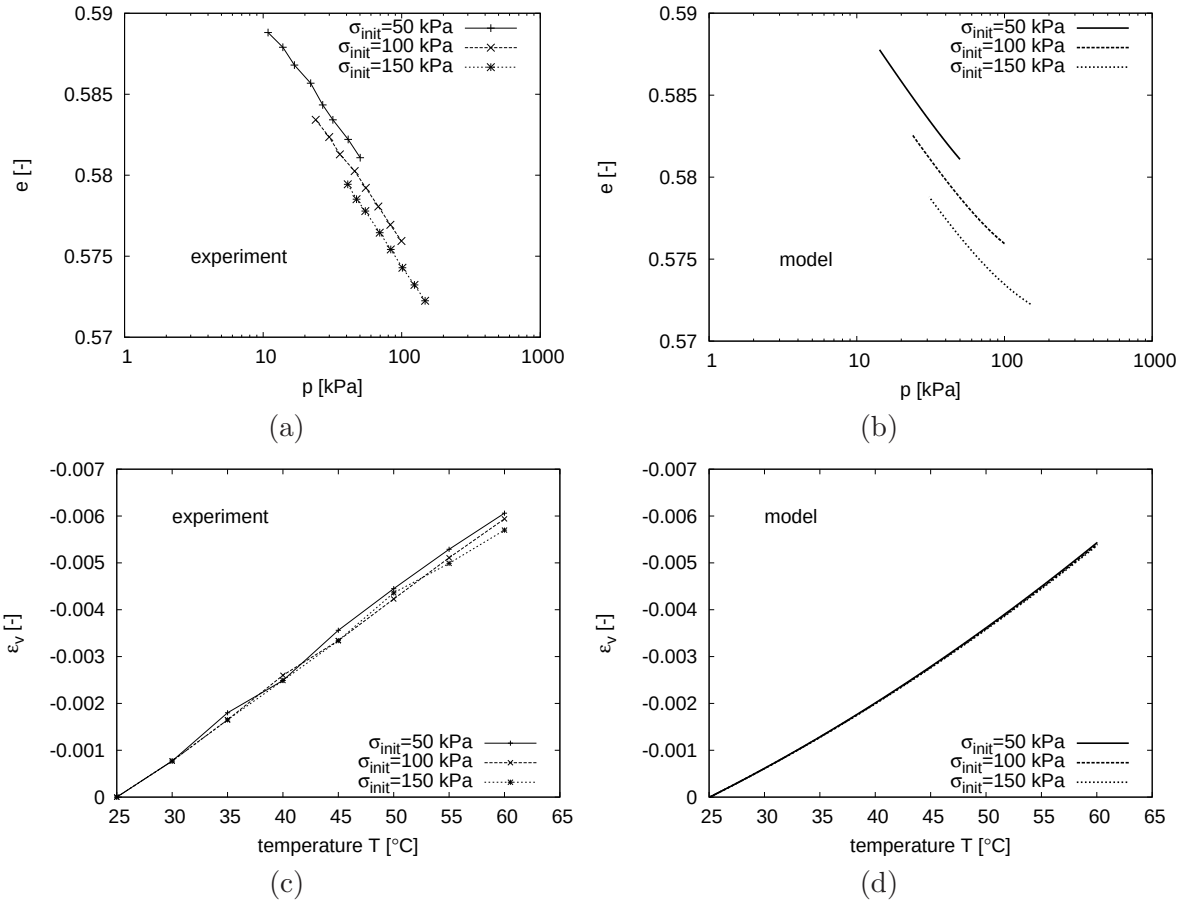

Figure 14: Experimental results (left) and model predictions (right) of void ratio and volumetric strain change during constant-water-content (undrained) heating experiments on saturated soil at different initial effective stresses (OCRs).

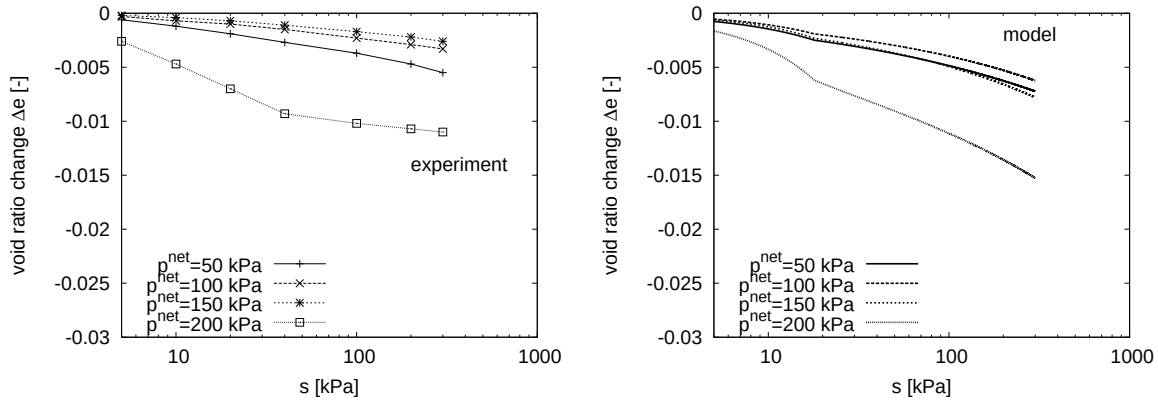

(a) (b)

Figure 15: Volumetric change due to suction increase in desaturation experiments at $T = 25°C$. (a) experiment, (b) model.

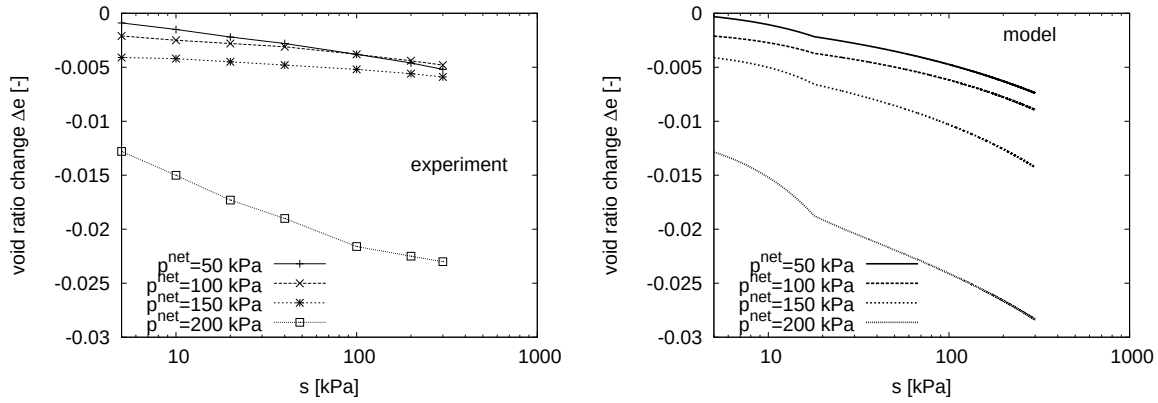

(a) (b)

Figure 16: Volumetric change due to suction increase in desaturation experiments at $T = 60°C$. (a) experiment, (b) model.

List of Tables

Table 1: *Parameters of the proposed model for the silt investigated by Uchaipchat and Khalili [69].*

Parameters of the basic model for saturated soils at the reference temperature	φ_c	λ^*	κ^*	N	r
	29.5°	0.06	0.002	0.772	0.2
Reference values of suction and temperature	s_e	T_0			
	18 kPa	$25°C$			
Parameters controlling the dependency of NCL on T and s	n_s	l_s	n_T	l_T	
	0.0035	0	-0.01	0	
Other parameters controlling wetting-drying and heating-cooling response	α_s		m		
	3.5×10^{-5}	$°C^{-1}$	2.5		